Journal of Asian Earth Sciences 165 (2018) 270–284

Contents lists available at ScienceDirect

Journal of Asian Earth Sciences

journal homepage: www.elsevier.com/locate/jseaes

Geology, Re-Os and U-Pb geochronology and sulfur isotope of the the Donggebi porphyry Mo deposit, Xinjiang, NW China, Central Asian Orogenic Belt

Chunming Han[a,b,*], Wenjiao Xiao[a,b], Benxun Su[a], Patrick Asamoah Sakyi[c], Songjian Ao[a], Jien Zhang[a], Zhiyong Zhang[a], Bo Wan[a,b], Dongfang Song[a], Zhongmei Wang[a], Na Zhao[a]

[a] Key Laboratory of Mineral Resource, Institute of Geology and Geophysics, Chinese Academy of Sciences, Beijing 100029, China
[b] CAS Center for Excellence in Tibetan Plateau Earth Sciences, Beijing 100101, China
[c] Department of Earth Science, University of Ghana, P.O. Box LG 58, Legon-Accra, Ghana

ARTICLE INFO

Keywords:
Re-Os
U-Pb
The Donggebi porphyry Mo deposit
Eastern Tianshan Orogenic Belt
Central Asian Orogenic Belt

ABSTRACT

The the Donggebi porphyry Mo deposit in the eastern section of the Eastern Tianshan Orogenic Belt in the Central Asian Orogenic Belt contains Mo metal reserves of 0.5 Mt. The deposit is hosted in Early Carboniferous metasedimentary rocks, namely; metasandstone, meta-sandy mudstone . Multiple hydrothermal activities have resulted in propylitic, phyllic, and argillic alteration in this deposit. Four stages (I-IV) of hydrothermal activity are identified. Stage I is represented by a mineral assemblage of K-feldspar, quartz and wolframite. Stage II consists of quartz + magnetite + pyrite ± chalcopyrite veinlets/veins with phyllic halos. Stage III consists of quartz + molybdenite + pyrite ± galena ± sphalerite ± chalcopyrite veins that are commonly related to phyllic alteration in the altered rocks. Stage IV has an assemblage of calcite + gypsum. Molybdenite mainly occurs in Stages III. Re-Os dating results for molybdenite samples from these two stages yielded an isochron age of 234.2 ± 1.6 Ma (2σ, MSWD = 0.25, n = 8). Porphyritic granites have a SIMS U-Pb zircon age of ~236 Ma and it was probably related to the Triassic felsic magmatism in this area. Values of $\delta^{34}S$ of sulfides range from 1.5‰ to 3.8‰, with an average value of 2.81 ± 2.24‰ (n = 22), reflecting a deep sulfur source. Most molybdenite samples have high $\delta^{34}S$ values (≥3.36‰) relative to other sulfide minerals (i.e., pyrite and chalcopyrite) of Stages I to III ($\delta^{34}S$ = 1.5–3.8‰, n = 18). Based on the geological history and spatial-temporal distribution of the granitoids, it is proposed that the Mo deposits in the eastern part of the East Tianshan Orogenic Belt formed in a post-collision extensional setting in the Early Mesozoic.

1. Introduction

The the Donggebi porphyry Mo deposit is located in the eastern section of the Eastern Tianshan Orogenic Belt of northwest China (Fig. 1). The Eastern Tianshan Orogenic Belt is considered to be the southernmost segment of the Central Asian Orogenic Belt (Xiao et al., 2004a,b, 2009), which is also known as the Altaid tectonic collage (Şengör et al., 1993). The Central Asian Orogenic Belt was formed mainly as a result of progressive subduction of the Paleo-Asian Ocean and amalgamation of various arcs and terranes during the Paleozoic (e.g., Şengör et al., 1993; Xiao et al., 2003a,b; Windley et al., 2007). It is characterized by extensive juvenile crustal growth from the Phanerozoic to Mesozoic (e.g., Jahn et al., 2000; Wu et al., 2000, 2002; Kovalenko et al., 2004). The Central Asian orogenic belt is also one of the three important metallogenic belts in the world and hosts numerous Cu, Ni, Fe, Au, Ag, Mo,W, Pb and Zn ore deposits, ranging in age from Neoproterozoic to Cretaceous (e.g., Zhang et al., 1999; Xiao et al., 2003a,b, 2009; Berzina et al., 2005; Han et al., 2006; Shen et al., 2012; Goldfarb et al., 2013; Seltmann et al., 2014;Chen et al., 2017; Wu et al., 2017a,b).

The Eastern Tianshan metallogenic domain in northwestern China forms a significant part of the Central Asian Orogenic Belt, one of the giant metallogenic belts in the world (e.g., Xiao et al., 2004a,b; Han et al., 2006; Shen et al., 2012; Seltmann et al., 2014; Chen et al., 2017;Wu et al., 2017a,b). The Central Asian Orogenic Belt bears one of the most important porphyry Cu ± Au ± Mo metallogenic provinces in the world (Seltmann and Porter, 2005; Gao et al., 2018; Fig. 1). Located on the northern margin of the Tarim Craton, the Chinese East Tianshan is the easternmost segment of the Tianshan Mountain Range in the southern Altaids (Xiao et al., 2004a,b). The East Tianshan

* Corresponding author at: Key Laboratory of Mineral Resource, Institute of Geology and Geophysics, Chinese Academy of Sciences, Beijing 100029, China.
E-mail address: cm-han@mail.iggcas.ac.cn (C. Han).

https://doi.org/10.1016/j.jseaes.2018.05.001
Received 16 November 2017; Received in revised form 1 May 2018; Accepted 2 May 2018
Available online 03 May 2018
1367-9120/

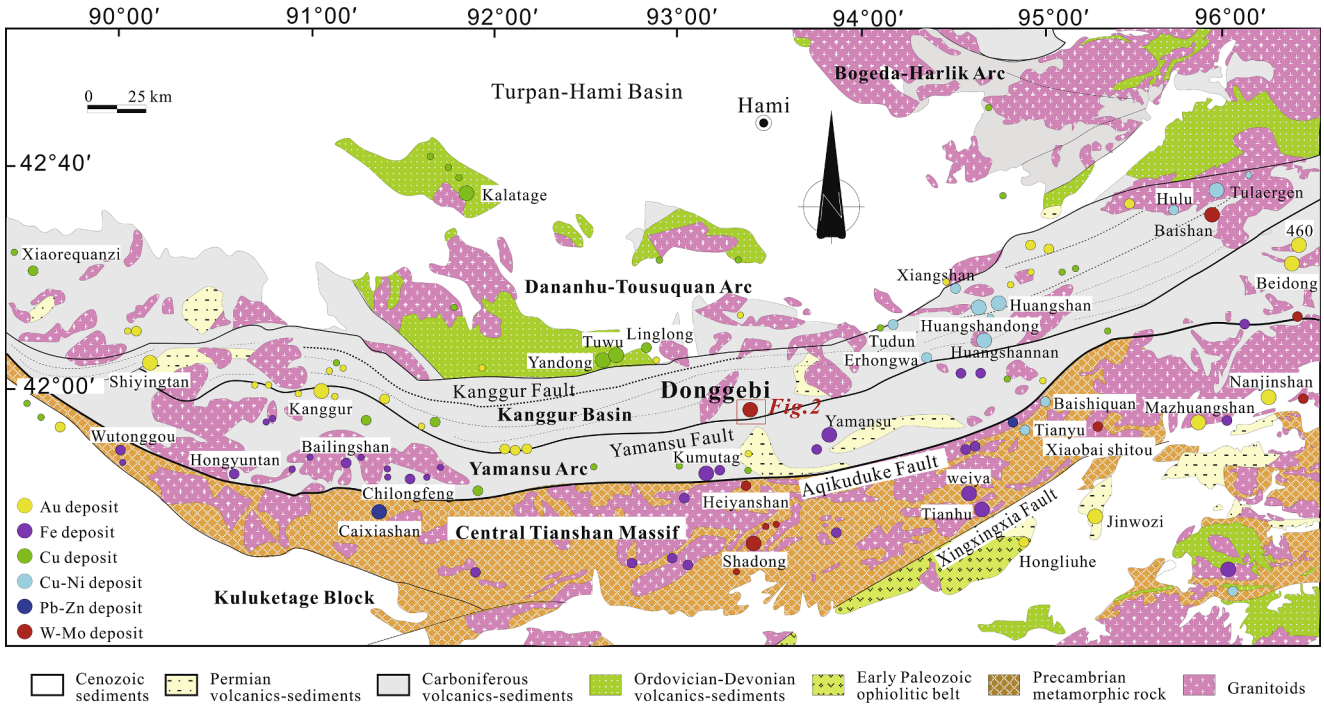

Fig. 1. Tectonic setting and distribution of significant deposits of the Eastern Tianshan Orogenic Belt, NW China (modified after Han et al., 2010; Deng et al., 2017).

polymetallic belt is one of the important producers of Cu–Au–Ni–Fe–Ag in China (Han et al., 2006; Fig. 2). The porphyry Cu deposits were considered to be related to the late evolutionary stages of a subduction-related oceanic or continental magmatic arc (Mao et al., 2011). The province also contains post-collisional metallic mineral deposits formed between 280 and 240 Ma (Zhang et al., 2005a,b).

The Donggebi is the largest, and economically the most important, deposit in the Eastern Tianshan Orogenic Belt, with total Mo metal reserves of 0.50 Mt (Huang et al., 2011a). It was discovered in 2008 and explored during the period 2009–2010; construction of the now-operating mine began in 2011. Since the discovery of the deposit, many scientific studies have been conducted that have addressed the geology and geochemistry of the deposit (Wang, 2011; Tu et al., 2011; Huang et al., 2011a,b; Wu et al., 2017a,b), as well as the geological and geochemical characteristics of the ore-forming granite porphyry (Yang et al., 2011; Deng, 2012). However, the documentation of the Donggebi deposit has been reported in the Chinese literature, and therefore the international geological community knows little about this deposit until now. In this contribution, we provide a detailed description of the the Donggebi Mo deposit, together with new molybdenite Re-Os and zircon U-Pb ages and S isotope compositions. Our results will be used to constrain the timing of mineralization and possible sources of sulfur and metals of the the Donggebi deposit.

2. Regional geological setting

The Eastern Tianshan Orogenic Belt (Fig. 1) contains a number of Paleozoic terranes that amalgamated between the Siberian and Tarim cratons, and underwent complex tectonic evolution (Coleman, 1989; Windley et al., 1990; Şengör et al., 1993; Şengör and Natal'in 1996; Xiao et al., 2004a,b). The tectonic history of the eastern Tianshan orogenic belt is considered to have been associated with the evolution of an ancient Tianshan ocean between the Tarim craton and the Junggar-Kazakhstan block (Allen et al., 1993; Şengör et al., 1993; Şengör and Natal'in 1996; Xiao et al., 2004a,b;Deng et al., 2016, 2017). The orogen is separated from the Tarim craton to the south by the Kanggguer ductile suture zone, and extends west to Gansu Province. The main structures of East Tianshan is characterized by a series of approximately east-west-trending faults, including the regional-scale Kalamaili-Maiqinwula, Kanggur, Yamansu, Aqikuduke and Xingxingxia faults, and many small-scale faults (Fig. 1; He et al., 1994; Xiao et al., 2004a,b). Of these faults, the Kangguer fault is the most prominent one, consisting of mylonite, tectono-clastic rocks, tectonic lenses, and breccia, and which not only forms the boundary between the Kazakhsta-Juanggar block and the Tarim craton, but is also an important structural zone along which major magmatic activities and associated ore mineralization took place (He et al., 1994).

Two distinct belts separated by the Kangguer fault can be recognized. The belt located north of the Kangguer deep-crustal fault is interpreted as an arc, named the Dananhu-Tousuquan magmatic arc (He et al., 1994; Ji et al., 1994; Guo, 2000), which consists mainly of Middle Devonian to Carboniferous volcanic rocks, and contains several porphyry Cu deposits of different sizes, including the Yandong, Tuwu, Linglong and Chihu deposits (Fig. 1; Zhang et al., 2002). The southern belt is located between the Kangguer and Aqikekudouke faults, and is also interpreted as an arc, named Aqishan-Yamansu magmatic arc (Ji et al., 1994; Ma et al., 1997), which consists of Carboniferous rocks along the northern side of the Tarim craton, including the Early carboniferous Aqishan and Yamansu Formations, and gray-wackes of the Middle Carboniferous Kushui Formation, separated by the Yamansu (or Kushui) Fault. It hosts numerous Fe, Cu, Au and Ag ore deposits. Representative of these are the Yamansu volcanic Cu–Fe deposit, the Weiquan Cu–Ag skarn deposit and the Lubaishan volcanic Cu deposit (Fig. 1).

The Kangguer fault separates Aqishan-Yamansu arc from the Tousuquan-Dananhu magmatic arc to the north, and is considered to represent a Late Carboniferous to Early Permian suture, along which folding and thrusting within the arc sequences occurred during the subduction of a Paleo-Tianshan ocean (Ji et al., 1994; Ma et al., 1997; Mao et al., 2002;Wu et al.,2014). By the end of the Carboniferous, an extensional tectonic regime developed along the major faults and the Kangguer orogenic lode deposits formed along some brittle-ductile shear zones within subordinate faults, which represent dilatational zones that were opened along an east-west-trending extension (Mao et al., 2002).

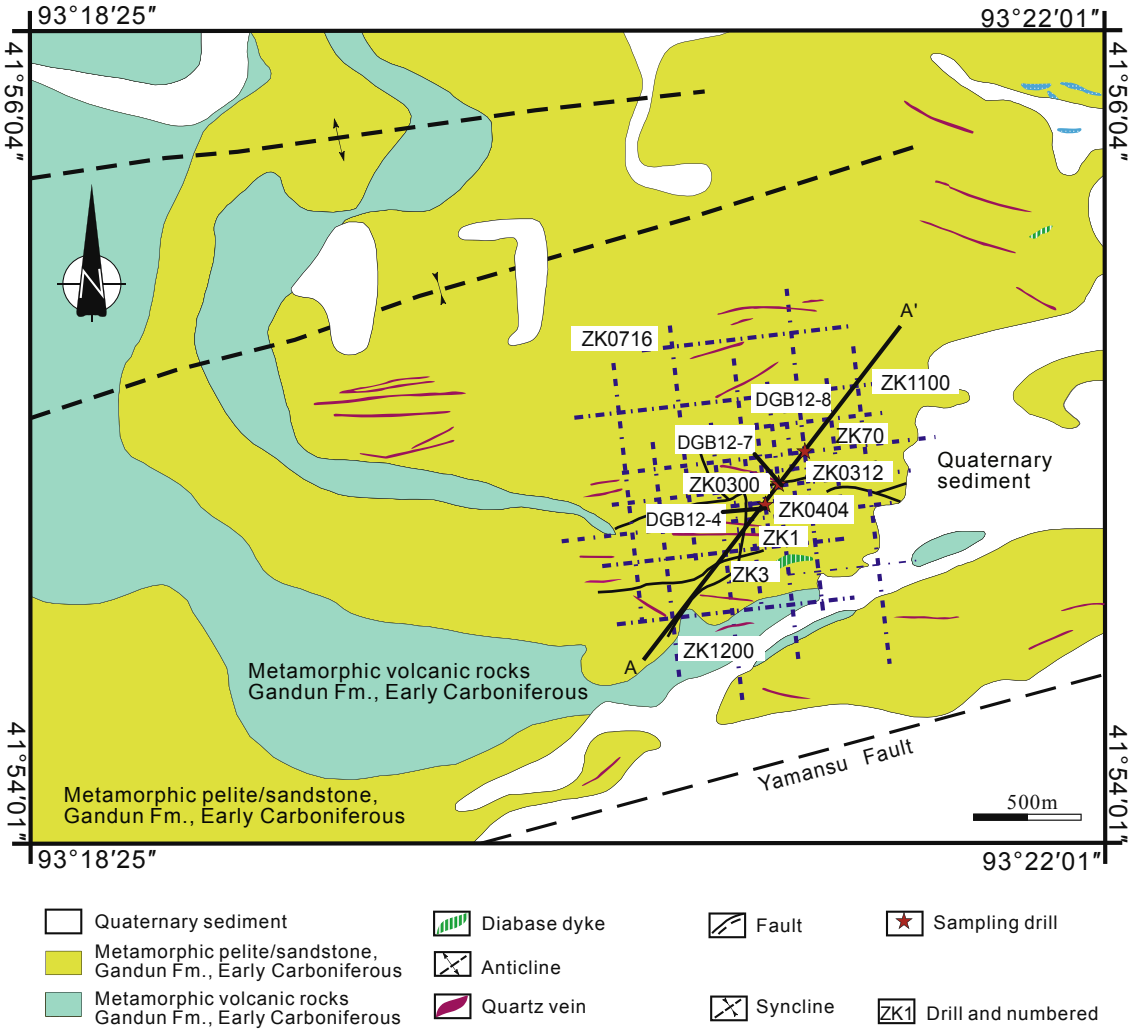

Fig. 2. Geological map of the the Donggebi Mo deposit (After Deng, 2012).

3. Deposit Geology

The Donggebi deposit is mostly concealed by Quaternary overburden and is mainly hosted in the Lower Carboniferous Gandun Formation (Fig. 2). The Gandun Formation is composed of meta-sandstone, meta-sandy mudstone, meta-argillaceous sandstone, meta-mudstone, silicalite, tourmalite, meta andesite, tuff and hornfels. The stratigraphic units trend WNW and dip ENE with an angle of 50–75°. The sedimentary rocks are thermometamorphically overprinted by deeper-seated intrusive rocks.

No intrusions are exposed at surface near the deposit, but several intrusive stocks and/or dikes, including porphyritic granite, granite porphyry, have been intersected in drill holes. Some granite porphyries occur as dikes in the mineralized area. An unmineralized biotite granite is emplaced in the northwestern part of the mining area. The Donggebi intrusion is composed of porphyritic granite and granite porphyry (Fig. 4). The coarse-grained porphyritic granite generally contains 2–9% orthoclase, 6–51% plagioclase, 20–35% quartz, and 1–3% biotite, with minor amounts of muscovite and sericite. Plagioclase crystals are often replaced by granular saussurite and fine-grained clay minerals. The granite porphyry generally contains 30% orthoclase, 40% plagioclase, 25% quartz, and 5% biotite, with minor amounts of apatite, muscovite and chlorite. The orthoclase crystals range from 0.51 to 1.00 mm in size. Alteration mineral include saussurite, sericite and chlorite. A zircon SHRIMP U-Pb age of 227.6 ± 1.3 Ma recently obtained from a porphyritic granite (Huang et al., 2011a). A stratabound-fracture zone is recognized, hosting the main mineralization, which trends NE and dip southeast with an angle of 30–60° (Fig. 3).

A total of five mineralized bodies have been identified, and they are distributed in the contact zone between porphyritic granite and meta-sedimentary rocks of the Lower Carboniferous Gandun Formation. Individual ore bodies vary from 280 m to 851 m in length and 10 m to 64.7 m in thickness. In the dipping direction, the explored ore bodies extend over 319 m below the surface (Fig. 3). The main ore bodies trend in NE direction with a dip angle of about 30° (see Fig. 4).

Principal metallic minerals are molybdenite and pyrite with minor quantities of chalcopyrite, galena, magnetite, scheelite and wolframite (Fig. 5). The gangue minerals include mainly orthoclase, plagioclase and quartz, with lesser amounts of calcite, muscovite and chlorite. The size of the molybdenite ranges from 0.03 mm to 3.00 mm. The ores are characterized by euhedral and subhedra textures, veinlet-disseminated and brecciated structures (Fig. 6)

Based on chemical and mineralogical analyses, several stages of hydrothermal alternation are recognized at the Donggebi. The highest Mo values occur in zones with complex hydrothermal overprinting. A potassic alternation (K-fsp + secondary biotite) affected the entire mineralized area. It involved microcline growth in the matrix around and between biotite and plagioclase. Minor discrete disseminated pyrite and magnetite, and veinlets of magnetite ± pyrite are present in the potassic alternation zones (see Fig. 7).

Light-coloured, almost white, irregular, phyllic (quartz-sericite/muscovite) alternation zones, overprint potassic alternation where

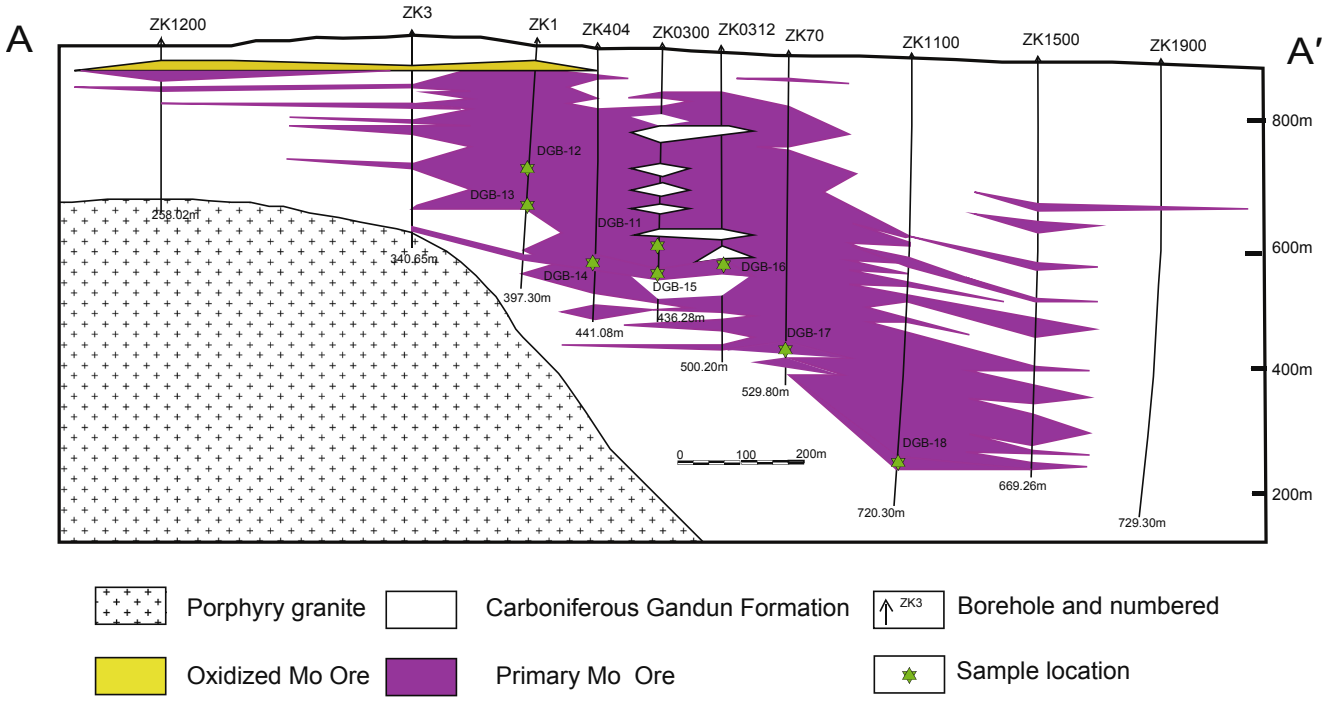

Fig. 3. Geological profile map of the the Donggebi Mo deposit (After Deng, 2012).

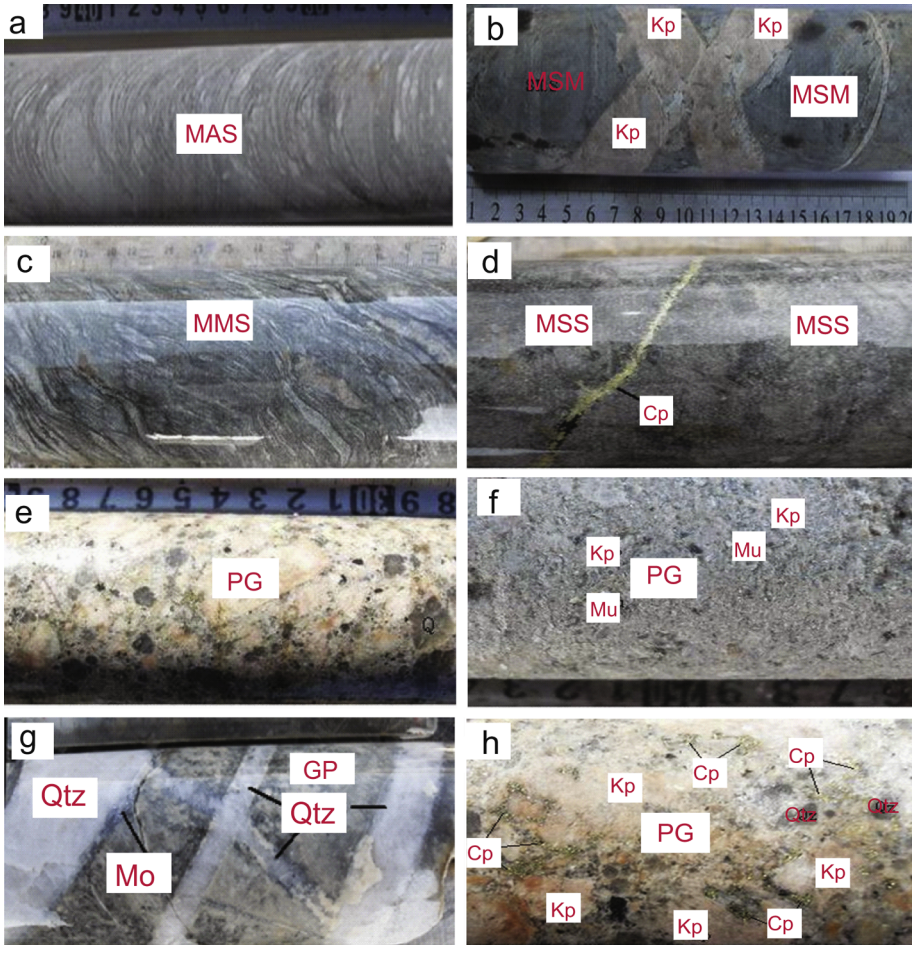

Fig. 4. Photographs of host rocks from the the Donggebi deposit. (a) Meta-sandly mud (drill hole ZK0303, depth 272 m); (b) Meta-argillaceous sandstone (drill hole ZK0302, depth 160.40 m); (c) Meta-mudstone (drill hole KZK0404, depth 26.00 m); (d) Meta-sandstone (drill hole KZK1108, depth 77.00 m); (e) Propylitic altered porphyritic granite (drill hole ZK0102, depth 540 m); (f) Muscovitization porphyritic granite (drill hole ZK0804, depth 184.80 m); (g) K-feldspar-quartz veinlet bearing granite porphyry (drill hole KZK0404, depth 179.48 m); (h) K-feldspar-quartz-chalcopyrite-bearing muscovitization porphyritic granite (drill hole ZK0102, depth 540 m); Abbreviations. Kp = K-feldspar phenocryst, Mu = muscovite, Mo = Molybdenite, Cp = Chalcopyrite, Quartz, PG = porphyritic granite, MSM = Meta sandy mud, MSS = Metasandstone, MAS = Meta argillaceous, MMS = Meta-mudstone.

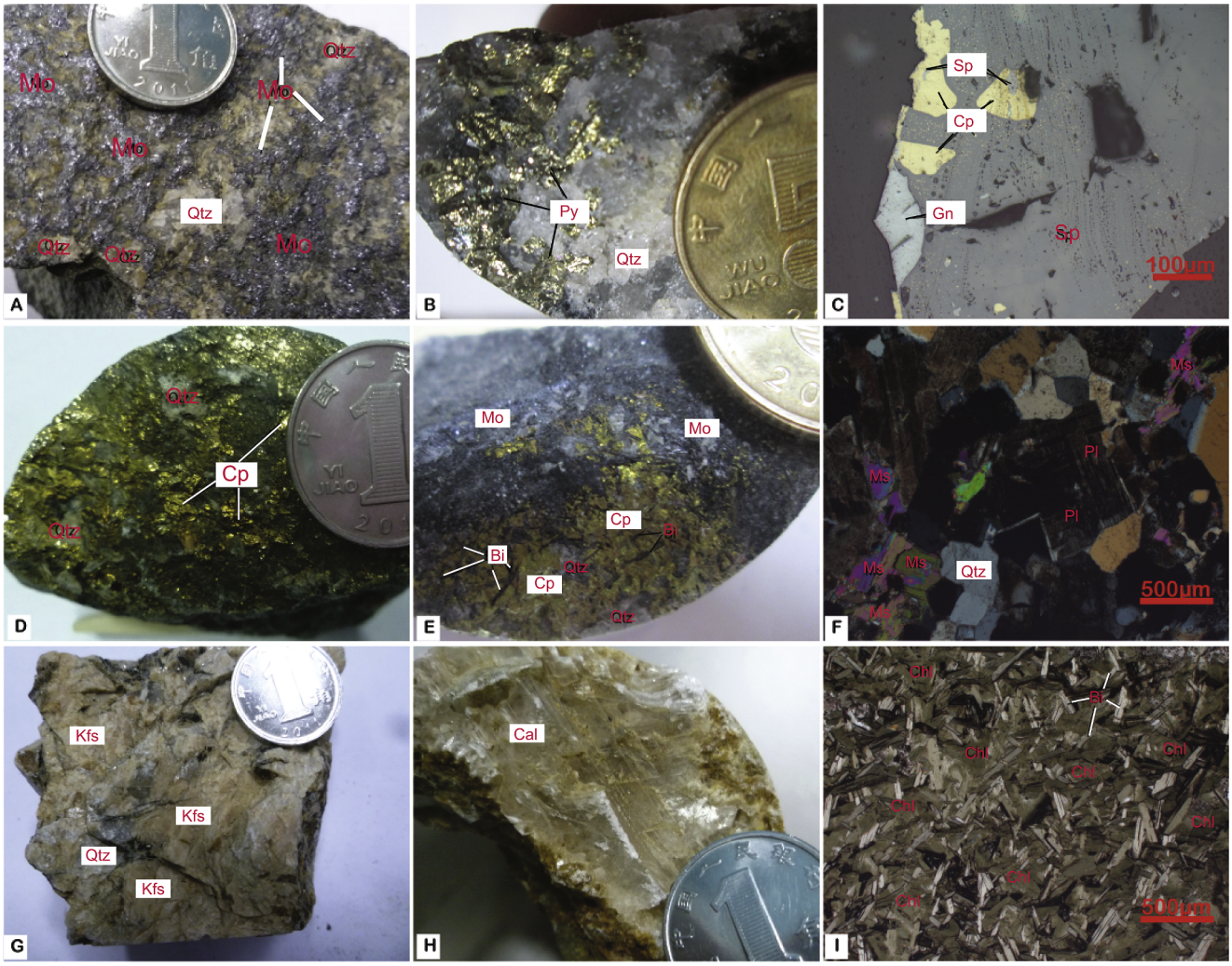

Fig. 5. Photographs of some ore samples from the the Donggebi Mo deposit. (A) Molybdenite veinlets in quartz; (B) Massive pyrite in quartz; (C) Disseminate chalcopyrite-sphalerite-galena in quartz vein; (D) Massive chalcopyrite in quartz; (E) Massive chalcopyrite-molybdenite in meta-sandstone; (F) Quartz, muscovite and polysynthetic twin plagioclase of porphyritic granite, polarization microscope; (G) Quartz-potash feldspar vein; (H) Calcite-quartz vein; I-Chloritization biotite. Abbreviations. Mo = Molybdenite, Qtz = Quartz, Py = Pyrite, Gn = Galena, Sp = **S**phalerite Cp = Chalcopyrite, Bi = Biotite, Ch = Chlorite, MS = Muscovite, Kfs = K-fedspar, Cal = Calcite.

sericite/muscovite together with fine-grained quartz have replaced feldspar. Euhedral pyrite is common in this zone, whereas minor chalcopyrite occurs with disseminated molybdenite. Silicification (silica flooding) with fine-grained quartz is associated with stockwork quartz veins and veinlets with chalcopyrite, pyrite, molybdenite, and magnetite. Weakly developed biotitization zone, related to late-stage vein composed of quartz and biotite and associated with minor Mo orebodies is hosted in this zone.

According to mineral assemblages and crosscutting relationships of the ore veins, five mineralization stages can be identified (Fig. 8). Stage I is characterized by K-feldspar and quartz veins; and wolframite also formed during this stage. Stage II is an assemblage consisting of quartz, magnetite, and a little molybdenite. Stage III (main mineralization stage) consists of molybdenite, chalcopyrite and pyrite, with minor galena and sphalerite. Stage IV is marked by the formation of the calcite and gypsum.

4. Samples and analytical methods

4.1. Re-Os molybdenite dating

We selected 8 samples from the Donggebi deposit for Re–Os dating, all of which were collected from ZK0404, ZK0300 and ZK0312. Sampling locations are marked in Fig. 2. Gravitational and magnetical separation was applied and then handpicked under a binocular microscope (purity > 99%). The molybdenite in the samples is fine grained (< 0.1 mm), thus avoiding the decoupling of Re and Os within large molybdenite grains (Stein et al., 1997).

Re-Os isotopic analyses were performed at the National Research Center of Geoanalysis, Chinese Academy of Geosciences. Details of the chemical procedure are giving in Du et al. (1995, 2001), Shirey and Walker (1995), Stein et al. (1997), and Markey et al. (1998) and are briefly described here.

The Carius tube (a thick-walled borosilicate glass ampoule) digestion technique was used. The weighed sample was loaded in a Carius tube through a long thin-neck funnel. The mixed ^{190}Os and ^{185}Re spike solution and 2 ml of 10 N HCl and 6 ml of 16 N HNO_3 were added while the bottom part of the tube was frozen at −80 to −50 °C in an ethanol-liquid nitrogen slush and the top sealed using an oxygen-propane torch. The tube was then placed in a stainless-steel jacket and heated for 10 h at 230 °C. Upon cooling, the bottom part of the tube was kept frozen, the neck of the tube was broken, and the contents of the tube were poured into a distillation flask after which the residue was washed out with 40 ml of water.

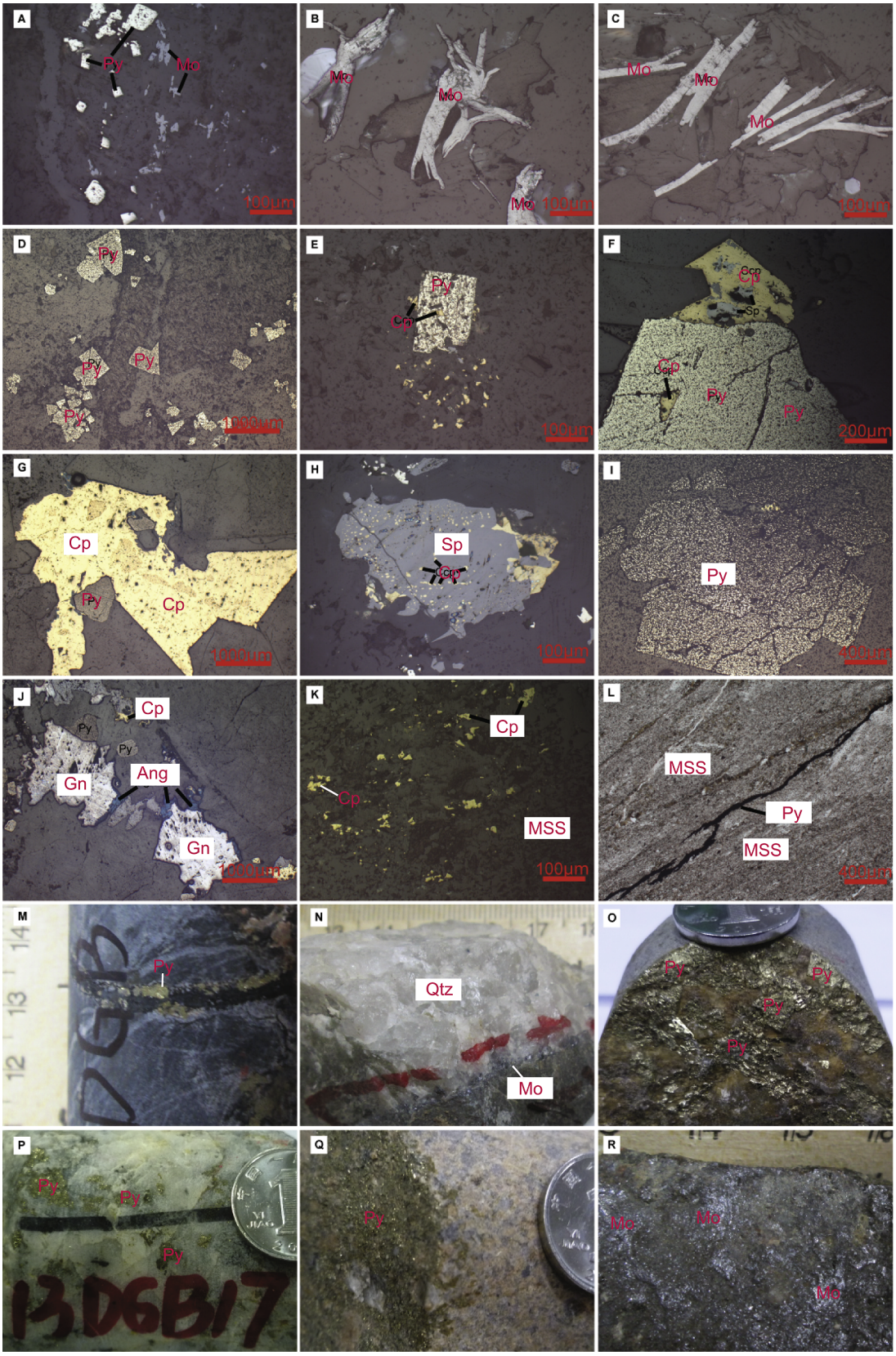

(caption on next page)

Fig. 6. Typical ore texture and structure in the the Donggebi Mo deposit. (A) Subhedral - allotriomorphic granular pyrite and allotriomorphic molybdenum; (B) Molybdenum vein presented in the quartz vein; (C) Foliated molybdenum occurred in the quartz vein; (D) Euhedral-subhedral granular pyrite; (E) Disseminated chalcopyrite and euhedral pyrite; (F) Massive ore sample consisting chalcopyrite and pyrite, and sphalerite vein present metasomatic structure in chalcopyrite; (G) Euhedral-subhedral granular pyrite and chalcopyrite in a eutectic texture; (H) Disseminated chalcopyrite occurring in the sphalerite, and some chalcopyrite present a euhedral-subhedral texture; (I) Euhedral pyrite in a cataclastic structure; (J) Galena and pyrite presented a eutectic texture; (K) Disseminated chalcopyrite in the metasandstone; (L) Pyrite veinlet in the metasandstone; (M) Occurrence of banded and massive pyrite in the meta-mudstone; (N) Molybdenum veinlet in a quartz vein; (O) Massive pyrite in the metasandstone; (P) Sparse disseminated pyrite occurring in quartz vein; (Q) Disseminated pyrite in the porphyritic granite; (R) Massive pyrite present in metasandstone. Abbreviations. Py = Pyrite, Mo = Molybdenite, Cp = Chalcopyrite, Sp = **S**phalerite, Qtz = Quartz, MSS = Metasandstone, Gn = Galena, Ang = anglesite.

Separation of osmium by distillation and separation of rhenium by extraction was performed based on the analytical method in Du et al. (2001). A TJA PQ-EXCELL ICP-MS was used for the determination of the Re and Os isotope ratio.

Average blanks for the total Carius tube procedure were ca. 10 pg Re and ca. 1 pg Os. The analytical reliability was tested by repeated analyses of molybdenite standard HLP-5 from a carbonatite vein-type molybdenum-lead deposit in the Jinduicheng-Huanglongpu area of Shaanxi Province, China. Fifteen samples were analyzed over a period of 5 months. The uncertainty in each individual age determination was about 0.35% including the uncertainty of the decay constant of 187Re, isotope ratio measurement, and spike calibrations. The average Re-Os age for HLP-5 is 221.3 ± 0.3 Ma (95% confidence limit, Stein et al. 1997). Median age and mean absolute deviation were 221.34 ± 0.12 Ma. The average Re concentration was 283.71 ± 1.54 μg/g, while the average Os concentration was 657.95 ± 4.74 ng/g.

4.2. Zircon U-Pb dating

Sample DGB12-4, DGB12-7 and DGB 12-8 are porphyritic granite, collected from the Donggebi porphyry Mo deposit, sample DGB12-4 (41°54′52″N, 93°20′43″E) collected from ZK0404, sample DGB12-7 (41°54′55″N, 93°20′45″E) collected from ZK0300 and sample DGB12-8 (41°54′58″N, 93°20′50″E) collected from ZK0312(Fig. 2).

Zircons were separated using conventional heavy liquid and magnetic techniques and picked under a binocular microscope. The grains were mounted along with Temora standard and then cast in epoxy resin in a 2.5 cm diameter mount and ground to expose the center of the grains. Internal structures of zircon were examined using cathodoluminescence (CL) images prior to U–Pb analyses. In-situ zircon U–Pb ages were acquired on the Cameca IMS-1280 ion microprobe (SIMS) in single collector mode at the Institute of Geology and Geophysics (IGG), Chinese Academy of Sciences, Beijing. The U–Th–Pb ratios and absolute abundances were determined relative to the standard zircon 91,500 (Wiedenbeck et al., 1995), analyses which were interspersed with those of unknown grains, using operating and data processing procedures similar to those described by Li et al. (2009). The mass resolution used to measure the Pb/Pb and Pb/U isotopic ratios was 5400 during the analyses. A long-term uncertainty of 1.5% (1RSD) for ^{206}Pb/238U measurements of the standard zircons was propagated to the unknowns (Li et al., 2010). Despite that the measured ^{206}Pb/^{238}U error in a specific session was generally around 1% (1RSD) or less. Measured compositions were corrected for common Pb using non-radiogenic ^{204}Pb. Corrections were sufficiently small to be insensitive to the choice of common Pb composition, and an average of present-day crustal composition (Stacey and Kramers, 1975) was used, assuming that the common Pb is largely surface contamination introduced during sample preparation. Uncertainties on individual analyses in data tables are reported at a 1σ level; mean ages for pooled U/Pb (and Pb/Pb) analyses are quoted with 95% confidence interval. Data reduction was carried out using the Isoplot/Ex v. 2.49 program (Ludwig 2001).

4.3. Sulfur isotope analyses

Twenty-two sulfide samples including molybdenite, pyrite and chalcopyrite were selected from different parts of orebodies for sulfur isotope analyses, there are collected from Stage III (main mineralization stage). Sulfide-bearing veins/veinlets were first cut from their host rocks and crushed to 40 to 80 mesh; sulfide minerals were then hand-picked under a binocular microscope to remove impurities. Sulfide separates were then crushed to < 200-mesh powder in an agate mortar. Sulfur isotope analyses were completed using a Finnigan MAT-252 mass spectrometer according to the method of Ueda and Sakai (1984), at the Institute of Geology and Geophysics, Chinese Academy of Sciences in Beijing. The sulfide powder was enclosed in a tin cup and then put in a reacting furnace. Subsequently, the powder was oxidized to SO_2(g). Helium was used as a carrier gas and mixed with SO_2 to facilitate transport into the mass spectrometer. Reference standards GBW04414 and GBW04415 were used as external standards to calibrate the sulfur isotope composition of unknown samples. During our analytical session, the obtained δ^{34}S values are −0.10 ± 0.17‰ (2σ; n = 12) for standard GBW04414, consistent with its recommended value of −0.07 ± 0.13‰ (2σ; Ding et al., 2001). The analytical precision is typically ± 0.2‰ (2σ).

5. Results

5.1. Re-Os molybdenite ages

The concentrations of Re and Os and the osmium isotopic compositions of molybdenite from the Donggebi Mo deposit are shown in Table 1. The total Re and Os concentrations of molybdenite range from 10 to 63 μg/g and 26 to 155 ng/g, respectively. Model ages for the deposit were calculated assuming that the initial abundance of ^{187}Os is zero. Isochron ages for all samples from the Donggebi Mo deposit were calculated using Isoplot Model 3 with 2% input error. The numbers within the brackets in Table 1 are measurement errors, and correspond to the last digit of analytical data in front of the brackets. A regression analysis was applied to 8 analytical data of molybdenite, which yields an isochron age of 234.3 ± 1.6 Ma (2σ) with an initial ^{187}Os of 0.04 ± 0.45 (MSWD = 0.25) (Fig. 9), identical to the mean age (234.4 ± 1.2 Ma, ± 0.50% 2σ, n = 8) calculated from the single sample age determination (Fig. 10). Model ages for individual analyses range from 233.7 ± 3.2 to 235.6 ± 3.4 Ma (Table 1).

5.2. Zircon U-Pb geochronology

Zircons from three samples of porphyritic granite were dated using the U-Pb technique in order to constrain the age of the main stage of magmatism. Fig. 10 shows representative cathodoluminescence (CL)-SEM images of zircon types from the porphyritic granite. The zircons have grain sizes from 50 μm to 200 μm. They are short, euhedral prisms, which in many cases have well-developed oscillatory zoning without distinctively older cores and younger overgrowths in the CL images (Fig. 10). SIMS zircon U-Pb data for the Donggebi intrusion are presented in the Table 2.

Thirty-nine analyses on 39 zircons from three samples (DGB12-4,

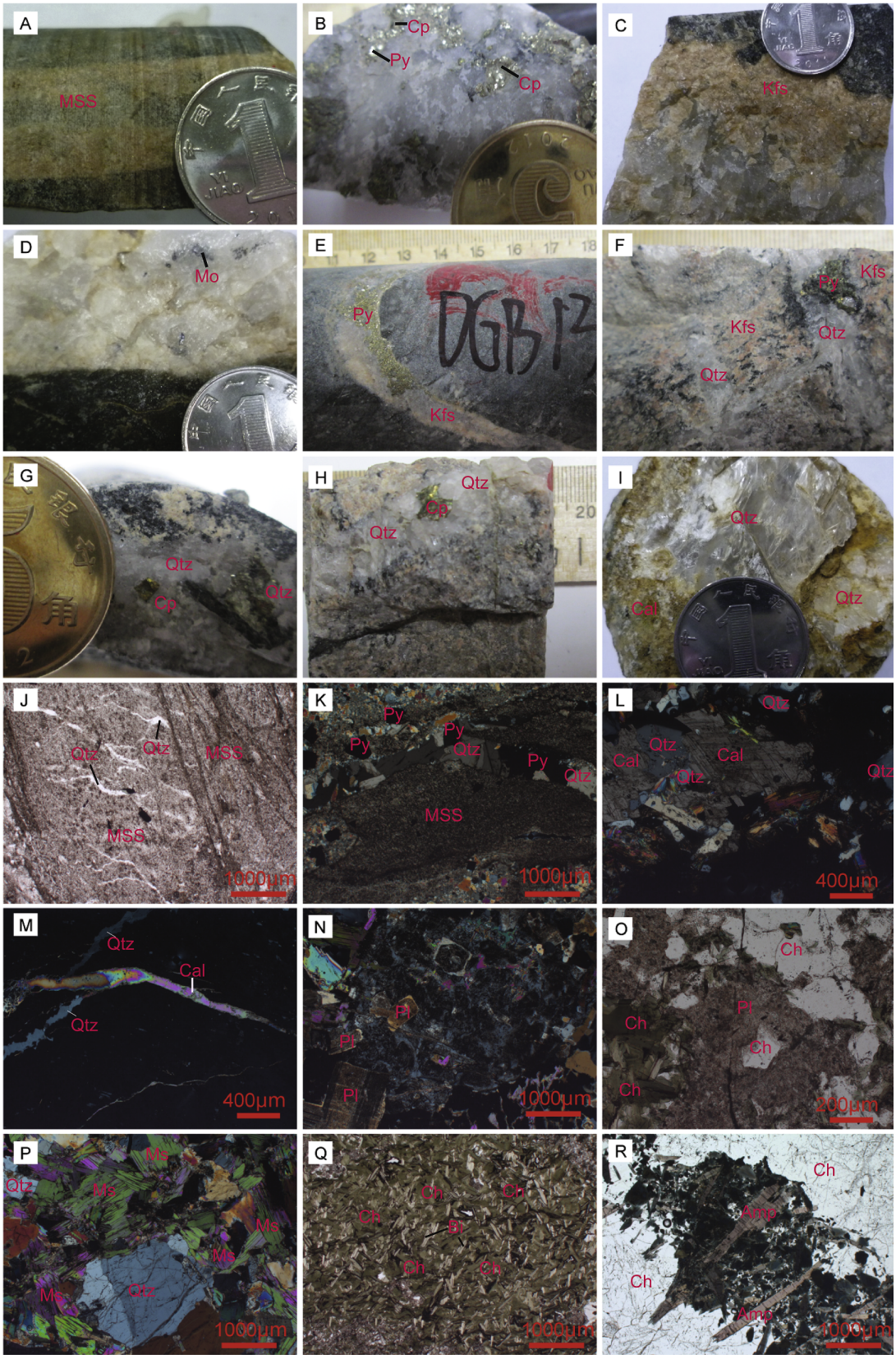

(caption on next page)

Fig. 7. Wall rock alteration in the the Donggebi Mo deposit. (A) K-feldspar alternation in the metasandstone; (B) Silicification, pyrite and chalcopyrite in quartz veins; (C) K-feldspar alternation and silicification in the metasandstone; (D) Silicification, disseminated molybdenite in quartz vein; (E) K-feldspar alternation and silification present in the metamudstone; (F) Silicification, the multi-phase quartz veins in the granite are interrelated with the fluorite vein ; (G) Silicification, fluorite-quartz veins developed in pyrite and chalcopyrite; (H) Silicification, the quartz vein in the porphyritic granite, and chalcopyrite in quartz vein; (I) Silicification and carbonatization, quartz - calcite vein present in the metasandstone; (J) Silicification, a quartz vein developed in metasandstone; (K) feldspar alternation and silification present in the metamudstone; (L) Silicification and carbonatization, quartz and calcite veins in the metamudstone; (M) Silicification and carbonatization, late calcite vein crosscutting earlier formed quartz vein; (N) Plagioclase with sericitization; (O) Metasandstone with sericitization; (P) Metamudstone with muscovite alternation and chloritizatio; (Q) Amphibole with chloritization. Abbreviations.Kfs = K-fedspar, Cp = Chalcopyrite, Py = Pyrite, Qtz = Quartz, MSS = Metasandstone, Cal = Calcite, Pl = Plagioclase, Ch = Chlorite, MS = Muscovite, Bi = Biotite, Amp = Amphibole, Mo = Molybdenite,

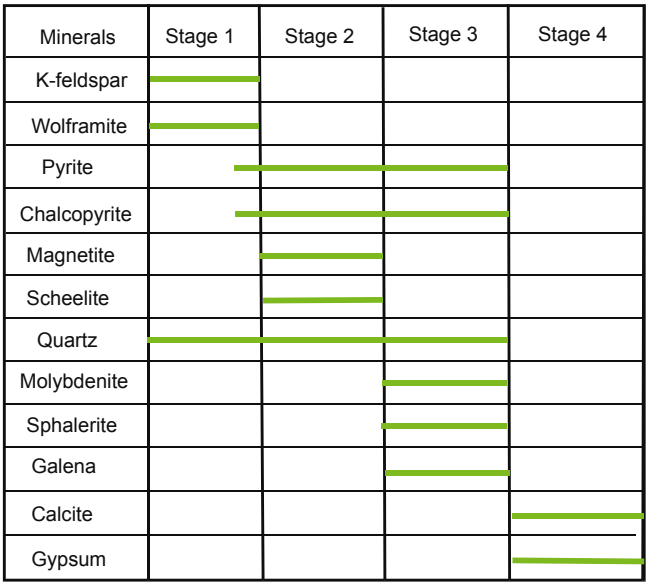

Fig. 8. Paragenesis sequence of minerals of the the Donggebi Mo deposit (modified from Deng, 2012).

DGB12-7, DGB12-8) were obtained. Zircons from the porphyritic granite are mostly euhedral and colourless. In CL images (Fig. 10), no inherited cores were observed. The zircons have high uranium (from 205 to 1647 ppm) and Th (from 108 to 1211 ppm) contents, and high Th/U ratios (from 0.40 to 1.38) (Table 2). Such features indicate that they were crystallized from magmas (Wu et al., 2006).

Fourteen spot analyses on 15 zircon grains from sample DGB12-4 yielded concordant $^{206}Pb/^{238}U$ ages that range between 239.0 ± 3.5 and 232.1 ± 3.5 Ma, with a weighted mean of 236.4 ± 2.7 Ma (95% confidence level, mean square weighted deviation [MSWD] = 0.36, n = 14; Fig. 11a). Fourteen spot analyses on 13 zircon grains from sample DGB12-7 yielded concordant $^{206}Pb/^{238}U$ ages that range between 239.5 ± 3.8 and 231.9 ± 3.4 Ma, with a weighed mean of 236.2 ± 3.3 Ma (95% confidence level, MSWD = 0.38, n = 14; Fig. 11b). Eleven spot analyses on 11 zircon grains from sample DGB12-8 yielded concordant $^{206}Pb/^{238}U$ ages that range between 238.6 ± 3.7 and 231.7 ± 3.4 Ma, with a weighed mean of 236.3 ± 3.2 Ma (95% confidence level, MSWD = 0.23, n = 11; Fig. 11c).

5.3. Sulfur isotope compositions of sulfide minerals

The $\delta^{34}S$ values of sulfides are presented in Table 3, and range from 1.5 to 3.8‰, with an average value of 2.81 ± 2.24‰ (n = 22), significantly higher than those of the mantle (0 ± 3‰) and most porphyry systems (0 ± 5‰), suggesting that a ^{34}S-enriched sulfur source contributed to at least part of the the Donggebi sulfur inventory. Eight molybdenite samples recorded a broad range of $\delta^{34}S$ values varying from 3.36 to 3.86‰ (n = 8, mean = 3.64 ± 0.11‰), whereas the ranges of $\delta^{34}S$ values for other sulfides are more restricted, i.e., 2.3 to 3.1‰ (n = 4, mean = 2.76 ± 0.31‰) for pyrite and 1.54 to 2.43‰ (n = 10, mean = 2.02 ± 0.35‰) for chalcopyrite.

6. Discussions

6.1. Source of ore-forming metals

It is well known that post-collisional granitoids form some of the largest volumes of granite in orogenic belts. Moreover, mantle sourced mafic magma contributions play an important role in their evolution. Recent studies show that I-type and A-type Central Anatolian granitoids are good examples of post-collisional granitoids in the Alpine orogenic belt and show geochemical evidence of mantle-derived mafic magma contributions (Delibaş, 2009; Delibaş et al., 2011). However, mafic magma contributions in the evolution of post-magmatic ore occurrences/deposits have not been known in the Central Asia Orogenic Belt. In recent years, the Re contents of the molybdenites have been used to trace the source of ore materials (Mao et al., 1999, 2003, 2006). The Rhenium content in molybdenites decreases gradually in the order; mantle source > a mixture of mantle and crust > crustal source (Mao et al., 1999, 2003, 2006). In addition, concluded that deposits with mantle components (e.g., mantle underplating, mantle metasomatism,

Table 1
Re-Os isotopic data for molybdenite from the Donggebi Mo deposit, easternTianshan.

No.samples	Weight (g)	$_{Re}$ (μg/g)		$^{187}_{Re}$(μg/g)		$^{187}_{Os}$(μg/g)		Model age (Ma)	
		Measured	2σ	Measured	2σ	Measured	2σ	Measured	2σ
DGB-12	0.02052	33.12	0.27	20.82	0.17	81.37	0.72	234.1	3.4
DGB-11	0.05034	41.97	0.31	26.38	0.19	103.8	0.90	235.6	3.4
DGB-13	0.05056	10.92	0.09	6.862	0.06	26.87	0.26	234.6	3.5
DGB-14	0.05018	38.24	0.32	24.03	0.20	93.91	0.78	234.1	3.3
DGB-15	0.05008	59.27	0.52	37.25	0.33	146.0	1.20	234.8	3.4
DGB-16	0.05012	41.03	0.34	25.79	0.21	101.0	0.80	234.7	3.3
DGB-17	0.05025	56.39	0.45	35.44	0.28	138.2	1.10	233.7	3.2
DGB-18	0.05015	63.18	0.56	39.71	0.35	154.9	1.30	233.7	3.4

Enriched ^{190}Os and ^{185}Re were obtained from the Oak Ridge National Laboratory. Decay constant:λ (^{187}Re) = 1.666 × 10^{-11}/year (Smoliar et al., 1996). The uncertainty in each individual age determination was about 0.35% including the uncertainty of the decay constant of ^{187}Re, uncertainty in isotope ratio measurement, and spike calibration.

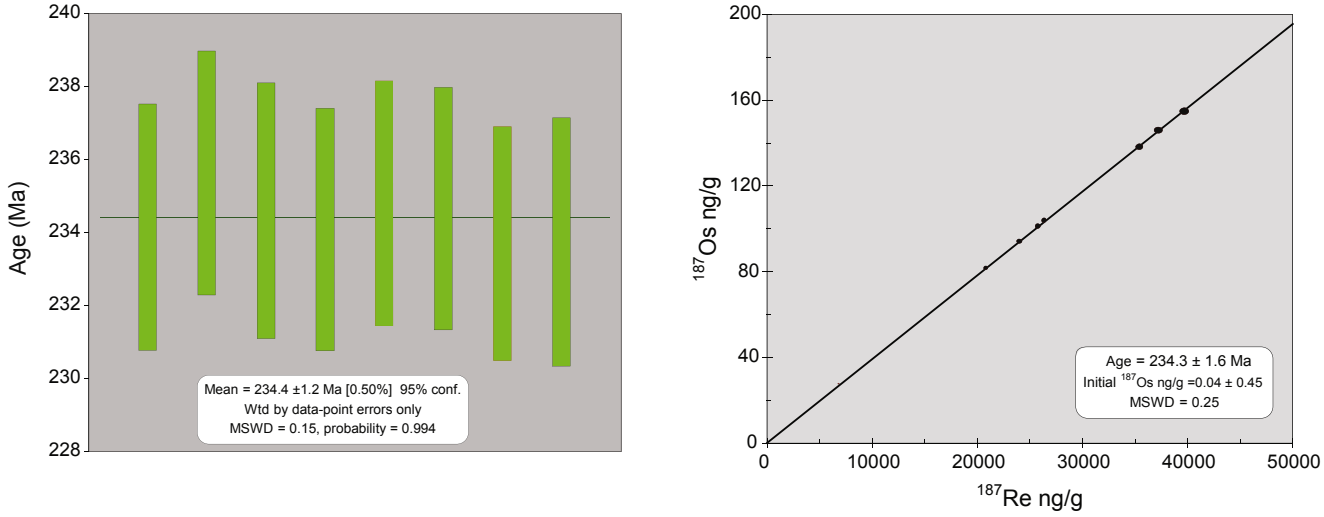

Fig. 9. (a) Re-Os weighted average model age diagram; (b) Isochron diagram for molybdenite samples from the the Donggebi Mo deposit. The Re-Os ages are listed in Table 2.

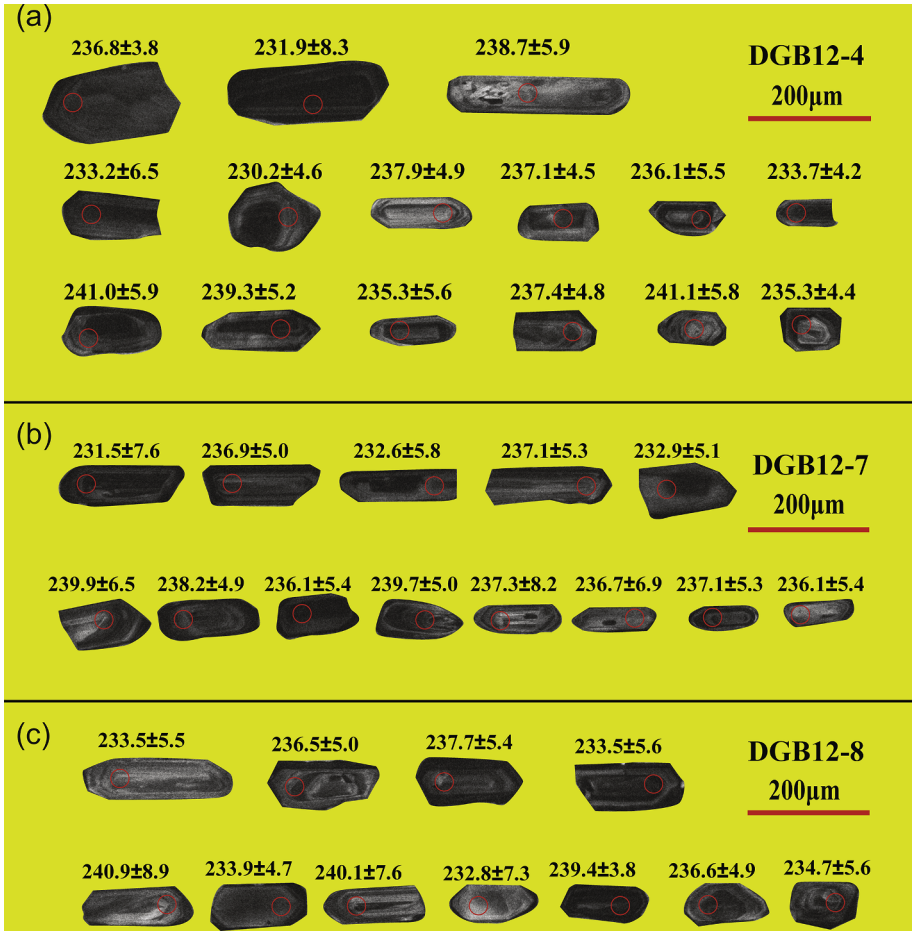

Fig. 10. Cathodolumninescence (CL) imagines of zircons from porphyritic granite of the Donggebi Mo deposit. Circles show the locations of SIMS U-Pb age isotope measurement, $^{206}Pb/^{238}U$(Ma) are shown above the circles. Numbers refer to spots listed in the Table 3. a-DGB-4, b-DGB-7, c-DGB-8,

melting of mafic or ultramafic rocks) have higher Re contents, whereas deposits of crustal origin have lower Re contents associated with molybdenites. In comparison to cited publications for different locations (e.g., Mao et al., 1999, 2003, 2005), the relatively lower Re contents of molybdenites from the Donggebi Mo deposit may indicate a mixed (crust + mantle) origin, but crustal components are more dominant.

In general, δ^{34}Ssulfide values for most porphyry-type deposits in the world range from −5 to 5‰, which are roughly consistent with the accepted mantle range (0 ± 3‰). Our results show that most of the sulfides from the Donggebi have $\delta^{34}S_{sulfide}$ lower than 5.0‰, and

Table 2
ZirconU-Pb data determined by monocollector SIMS mode of porphyritic granite from the Donggebi Mo deposit.

Sample spot	Th/(ppm)	U/(ppm)	Th/U	$^{207}Pb/^{206}Pb$	1σ	$^{207}Pb/^{235}U$	1σ	$^{206}P/^{238}U$	1σ	$^{207}Pb/^{206}Pb$	1σ	$^{207}Pb/^{235}U$	1σ	$^{206}Pb/^{238}U$	1σ
DGB12-4															
@1	960	1382	0.70	0.0519	1.01	0.2627	1.81	0.0367	1.50	283.0	23.0	236.8	3.8	232.2	3.4
@2	143	288	0.50	0.0498	3.65	0.2565	3.97	0.0374	1.57	186.0	82.8	231.9	8.3	236.4	3.6
@3	195	340	0.58	0.0509	2.26	0.2650	2.76	0.0378	1.58	236.3	51.3	238.7	5.9	238.9	3.7
@4	273	476	0.57	0.0509	2.71	0.2581	3.11	0.0368	1.51	234.8	61.5	233.2	6.5	233.0	3.5
@5	426	880	0.48	0.0502	1.67	0.2545	2.25	0.0368	1.50	202.6	38.4	230.2	4.6	233.0	3.4
@6	625	1037	0.60	0.0505	1.77	0.2640	2.32	0.0379	1.50	219.0	40.4	237.9	4.9	239.8	3.5
@7	349	580	0.60	0.0514	1.51	0.2631	2.13	0.0371	1.50	259.7	34.3	237.1	4.5	234.9	3.5
@8	470	539	0.87	0.0513	2.12	0.2617	2.60	0.0370	1.51	253.0	48.1	236.1	5.5	234.4	3.5
@9	614	1281	0.48	0.0508	1.24	0.2588	2.02	0.0370	1.60	229.5	28.3	233.7	4.2	234.1	3.7
@10	192	250	0.77	0.0516	2.29	0.2678	2.75	0.0377	1.52	266.2	51.7	241.0	5.9	238.4	3.6
@11	743	1245	0.60	0.0510	1.94	0.2657	2.45	0.0378	1.51	241.6	44.1	239.3	5.2	239.0	3.5
@12	443	553	0.80	0.0503	2.17	0.2608	2.64	0.0376	1.50	208.6	49.5	235.3	5.6	238.0	3.5
@13	683	728	0.94	0.0516	1.68	0.2634	2.28	0.0370	1.54	268.2	38.1	237.4	4.8	234.3	3.5
@14	233	342	0.68	0.0530	2.24	0.2680	2.70	0.0367	1.52	329.5	50.0	241.1	5.8	232.1	3.5
DGB12-7															
@1	108	289	0.38	0.0502	3.25	0.25603	3.67	0.0370	1.71	204.2	73.8	231.5	7.6	234.2	3.9
@2	219	256	0.85	0.0532	2.19	0.27112	2.73	0.0370	1.63	337.0	49.0	243.6	5.9	234.0	3.7
@3	179	390	0.46	0.0515	1.79	0.26276	2.34	0.0370	1.51	263.7	40.5	236.9	5.0	234.2	3.5
@4	236	519	0.45	0.0506	2.32	0.25745	2.77	0.0369	1.51	221.4	52.8	232.6	5.8	233.7	3.5
@5	130	207	0.63	0.0502	4.94	0.25334	5.16	0.0366	1.51	202.2	110.7	229.3	10.7	231.9	3.4
@6	198	318	0.62	0.0509	1.99	0.26298	2.51	0.0374	1.53	237.7	45.3	237.1	5.3	237.0	3.6
@7	686	497	1.38	0.0504	1.91	0.25780	2.43	0.0371	1.50	214.6	43.6	232.9	5.1	234.7	3.5

Sample spot	Th/ppm	U/ppm	Th/U	$^{207}Pb/^{206}Pb$	1σ	$^{207}Pb/^{235}U$	1σ	$^{206}P/^{238}U$	1σ	$^{207}Pb/^{206}Pb$	1σ	$^{207}Pb/^{235}U$	1σ	$^{206}Pb/^{238}U$	1σ
DGB12-7															
@8	308	373	0.82	0.0515	2.60	0.26651	3.01	0.0375	1.52	263.3	58.7	239.9	6.5	237.5	3.5
@9	308	573	0.54	0.0516	1.72	0.26439	2.29	0.0372	1.51	267.5	38.9	238.2	4.9	235.2	3.5
@10	206	347	0.59	0.0519	2.07	0.26177	2.56	0.0366	1.52	281.3	46.6	236.1	5.4	231.6	3.5
@11	238	425	0.56	0.0510	1.69	0.26629	2.33	0.0379	1.60	241.7	38.5	239.7	5.0	239.5	3.8
@12	136	257	0.53	0.0539	2.70	0.27407	3.17	0.0369	1.65	366.3	59.8	245.9	6.9	233.5	3.8
@13	212	355	0.60	0.0517	3.56	0.26322	3.87	0.0369	1.52	271.9	79.5	237.3	8.2	233.8	3.5
@14	212	402	0.53	0.0512	2.90	0.26248	3.27	0.0371	1.51	252.1	65.3	236.7	6.9	235.1	3.5
DGB12-8															
@1	385	568	0.68	0.0506	2.16	0.25855	2.64	0.0371	1.51	221.0	49.3	233.5	5.5	234.7	3.5
@2	443	839	0.53	0.0504	1.74	0.26226	2.35	0.0377	1.58	215.7	39.7	236.5	5.0	238.6	3.7
@3	275	509	0.54	0.0512	2.06	0.26375	2.55	0.0373	1.51	250.6	46.8	237.7	5.4	236.4	3.5
@4	295	540	0.55	0.0512	2.21	0.25852	2.69	0.0366	1.53	249.2	50.0	233.5	5.6	231.9	3.5
@5	130	225	0.58	0.0529	3.84	0.26777	4.12	0.0367	1.51	325.9	84.9	240.9	8.9	232.3	3.4
@6	518	826	0.63	0.0504	1.68	0.25905	2.26	0.0373	1.51	212.0	38.5	233.9	4.7	236.1	3.5
@7	181	256	0.71	0.0521	3.21	0.26681	3.55	0.0371	1.51	290.3	71.7	240.1	7.6	235.0	3.5
@8	177	244	0.73	0.0511	3.18	0.25770	3.52	0.0366	1.50	244.6	71.6	232.8	7.3	231.7	3.4
@9	1211	1647	0.74	0.0516	0.90	0.26588	1.78	0.0374	1.53	266.6	20.5	239.4	3.8	236.6	3.6
@10	294	737	0.40	0.0513	1.77	0.26234	2.32	0.0371	1.51	252.1	40.2	236.6	4.9	235.0	3.5
@11	458	556	0.82	0.0509	2.20	0.26008	2.67	0.0370	1.50	237.6	50.0	234.7	5.6	234.4	3.5

molybdenite and pyrite from early stages in the paragenesis (i.e., Stages II and III) generally have higher $\delta^{34}S_{sulfide}$ than those of pyrite and chalcopyrite from later stages. These relatively high $\delta^{34}S_{sulfide}$ values could either be inherited from the magmatic source, or resulted from contamination by crustal marine sedimentary facies or evaporites with high $\delta^{34}S_{sulfide}$ values. Due to the fact that no marine evaporites or carbonates have been reported near the Donggebi deposit, and that the Tuwu porphyry Cu deposit in this region has generally lower $\delta^{34}S_{sulfide}$ values (−0.9 to +1.3‰; Han et al., 2006), we therefore suggest that the relatively lower $\delta^{34}S_{sulfide}$ values of the sulfides from the Donggebi were probably inherited from a deep crustal material or the upper mantle.

6.2. Age of mineralization and its geological significance

The Re-Os geochronometer, applied to molybdenite, has been demonstrated to be remarkably robust, even in situations of overprint by metamorphism and deformation. If molybdenite does not contain any initial or common Os, all measured Os is monoisotopic (187Os) as the product of decay of 187Re, and the isochron age then represents the depositional age of molybdenite. For the Donggebi Mo ore deposit, the analysis of eight molybdenite samples yielded an isochron age of 234.3 ± 1.6 Ma (2σ) with an initial ^{187}Os of 0.04 ± 0.45. It is shown that the initial ^{187}Os values from the molybdenite samples are close to zero and the Re-Os isochron ages reflect the time of sulfide deposition. The Mo mineralization of the Donggebi Mo deposit took place after regional low-grade metamorphism and folding, and was not influenced by later geological events.

Mineralization in the eastern Tianshan, reported by some researchers (Mao et al. 2003; Han et al., 2010), is mainly of Late Paleozoic age (330–260 Ma). Younger mineralization ages from the Indosinian epoch (Mesozoic) have rarely been reported in the literature. However, recent studies indicate that the ages of the Jinwuozi gold deposit are 228–230 Ma, the Au-bearing quartz vein III of the Shiyingtan gold deposit is 244 ± 9 Ma, the Xiaobaishitou W-Mo deposit yield Re-Os isotope model ages range from 239.7 ± 3.6 Ma to 251.4 ± 3.6 Ma(Deng et al., 2017), and the Baishan Re-Mo deposit are between 225 and 233 Ma (Zhang et al., 2005a,b) .

Similarly, some ages of 244–215 Ma of metal deposits in the Beishan have been reported (Liu et al., 2003). These ages are close to the Re-Os

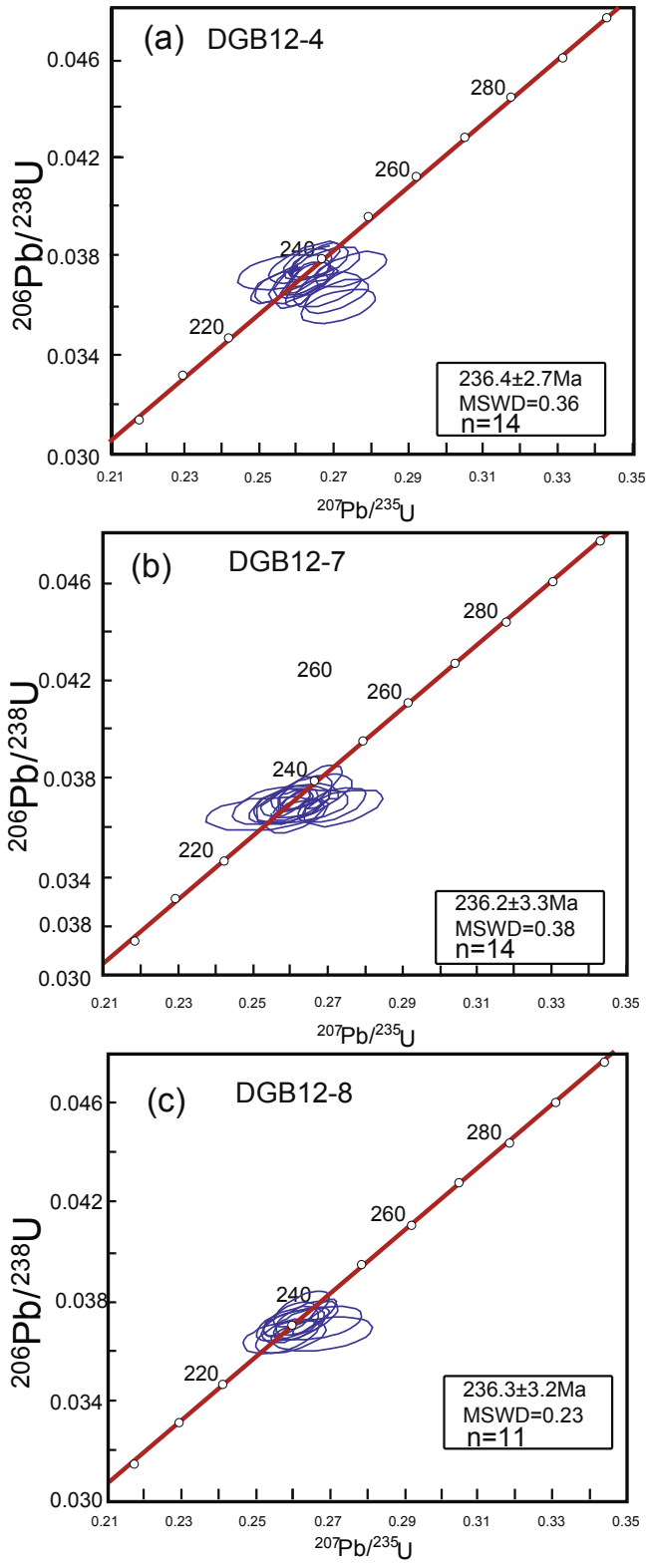

Fig. 11. Zircon U-Pb Concordia diagrams for the dated porphyritic granite of the Donggebi Mo deposit. (a) DGB-4, (b) DGB-7, (c) DGB-8,

ages (234 Ma) of molybdenite from the Donggebi Mo deposit in the eastern Tianshan, and indicate that the Indosinian period is also an important mineralization epoch in the eastern Tianshan orogenic belt.

6.3. Ore-forming geodynamical setting

Almost all porphyry-style deposits described in the literature are Phanerozoic and their formation is linked to magmatic activity at active plate margins. They can be divided into two main types. porphyry Cu-Mo and porphyry Cu-Au ± Mo deposits. The first type is generally found in continental margin arcs, like the Andean belt, dominated by calc-alkaline intrusions. The second type is typical of continental margins or island arc terranes, such as those in the southwest Pacific region where calc-alkaline rocks or high-K, calc-alkaline rocks prevail.

In the Rb against Y + Nb diagram (Fig. 12; Table 4), the Donggebi porphyritic granites mainly show post-COLG characteristics. In this case, ages of the Mo mineralization (234.3 ± 1.6 Ma) and also ages and tectonic setting of the host rocks (the Donggebi) reveal that Mo mineralization in the Eastern Tianshan Orogenic Belt occurred during the post-collisional setting. The Eastern Tiashan Orogenic Belt became Angaran active continental margin before the Early Permian (Xiao et al., 2004a,b). Its geodynamic evolution was closely associated with the evolution of an ancient Asian ocean, crustal thickening and compressional tectonics occurred at Late Permian times, and after the early Triassic time the thin-skin extensional tectonics continued to stretch the crust in the region (Xiao et al., 2004a,b).

Post-orogenic suites correspond to the last magmatic episodes in an orogenic belt. Structural data from Permian to Triassic rocks in regions adjacent to Eastern Tianshan indicate extensive thrusting, strike-slip faulting, and possibly also extension associated with the amalgamation of different blocks (Lamb et al., 2008; Laurent-Charvet et al., 2003; Wang et al., 2010). The existence of post-orogenic Triassic granitoids in the Eastern Tianshan near to the western part of the Beishan region has been used to support a change in geodynamic regime from Paleo-Asian Ocean subduction-collision to the Paleo-Tethys Oceanic regime which took place during the Late Permian to Early Triassic (Zhang et al., 2005a,b; Li et al., 2010). These regional studies reveal that the final amalgamation between the southern active margin of the Siberia Craton and the passive margin of Tarim Craton, may have extended from the end-Permian to Early Triassic (Xiao et al., 2004a,b). Therefore, we conclude that the mid-Triassic pluton in the Eastern Tianshan region was generated during this post-orogenic event.

Many Triassic plutons have been recognized from the eastern part of the CAOB and the northern parts of the North China Craton, and many of them are distributed along collision belts between the southern Mongolia arc terranes and the North China Craton (Chen et al., 2009; Li et al., 2010; Wu et al., 2011). Our study now shows that similar Triassic plutons are also present in the Eastern Tianshan orogen, indicating that Triassic magmatism extends into the south-central margin of the CAOB. Triassic magmatic activity may therefore be more widespread than previously considered.

In the CAOB, Triassic granitoids occur widely in the eastern segment, such as NE Mongolia, NE China and the Russian Far East (Transbaikalia), (Jahn et al., 2000, 2009; Wu et al., 2011; Yarmolyuk et al., 2002). These granitoids were predominately of *syn*-orogenic or post-orogenic types and most likely related to Mesozoic subduction/collision, such as the Transbaikal arc and Mongol-Okhotsk suturing, as well as the Circum-Pacific arcs (Yarmolyuk et al., 2002). In the central part of the CAOB, such as in central Mongolia (Jahn et al., 2009; Yarmolyuk et al., 2002), the Early to Middle Triassic intrusions were also probably emplaced in a *syn*-orogenic or postorogenic setting. This was related to the Mesozoic collision of the Baydrag and Hangay blocks and Mongol-Okhotsk suturing (Badarch et al., 2002; Orolmaa et al., 2008; Yarmolyuk et al., 2002). By contrast, further west in the CAOB, i.e., the Altai region, the Early Mesozoic granites were intruded in a post-orogenic to anorogenic setting (Wang et al., 2010). However, in the Beishan orogen located at the mid-southern margin of the CAOB, the Triassic plutons were mainly generated in a post-orogenic setting. Therefore, the Early to Middle Triassic granitoids in the western and eastern parts of the CAOB may record different tectonic settings (Li

Table 3
Sulfur compositions of sulfide minerals from the Donggebi Mo deposit.

Sample No.	Minerals	$\delta^{34}S_{CDT}$ (‰)	Sample No.	Minerals	$\delta^{34}S_{CDT}$ (‰)
DGB-02	Chalcopyrite	1.94	DGB-12	Pyrite	3.08
	Molybdenite	3.81		Chalcopyrite	2.14
DGB-03	Chalcopyrite	2.25		Molybdenite	3.75
	Molybdenite	3.78	DGB-13	Chalcopyrite	1.70
DGB-04	Chalcopyrite	2.04		Pyrite	2.84
	Molybdenite	3.61	DGB-14	Chalcopyrite	1.94
DGB-06	Chalcopyrite	2.22		Molybdenite	3.64
	Pyrite,	2.34	DGB-16	Chalcopyrite	1.98
	Molybdenite	3.57		Pyrite	2.78
DGB-09	Chalcopyrite	2.43	DGB-20	Chalcopyrite	1.54
	Molybdenite	3.57		Molybdenite	3.36

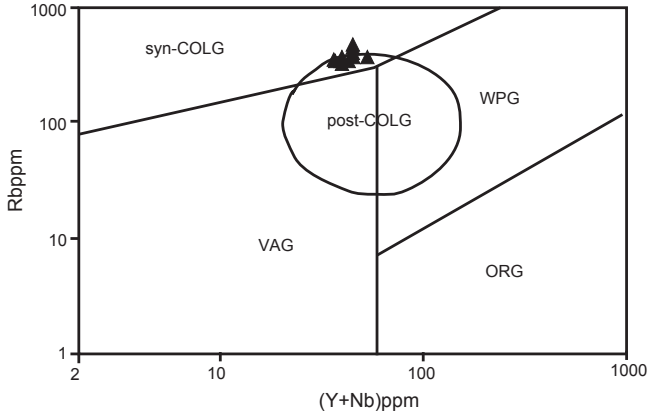

Fig. 12. The Rb against Y + Nb diagram of porphyritic granite from the the Donggebi Mo deposit. VAG = Volcano Arc Granite, Syn-COLG = Syncollision Granite, WPG = Within-Plate Granite.ORG = Ocean Ridge granite.

et al., 2010). In other words, voluminous *syn*-orogenic granitoids occur in the eastern part (and at the southeastern margin), whereas there is little anorogenic magmatism in the more western parts (and at the southwestern margin). This provides evidence that the final phase of Paleo-Asian Ocean closure of the CAOB took place a gradual scissor-type closure from west to east.

7. Conclusions

The Donggebi porphyry Mo deposit in the eastern Tianshan orogenic belt is hosted in the Lower Carboniferous Gandun Formation metasedimentary rocks. Five stages of mineralization are associated with propylitic and phyllic alterations. Molybdenite mainly occurs in veins and veinlets that contain quartz, fluorite, magnetite, and pyrite, with minor chalcopyrite, sphalerite, and galena, and is associated with phyllic alteration. Re-Os molybdenite dating results indicate that this deposit formed at ~234 Ma, whereas SIMS U-Pb zircon age of ~236 Ma for the porphyritic granite suggest that it was probably related to the Triassic felsic magmatism in this area. Sulfur isotope data for sulfide minerals, together with their paragenesis, suggest a mantle-

Table 4
Trace element compositions of porphyritic granite from the Donggebi Mo deposit.

Samples No.	DGB-1	DGB-2	DGB-3	DGB-4	DGB-5	DGB-6	DGB-7	DGB-8	DGB-9	DGB-10	DGB-11
La	19.2	22.4	21.5	20.8	24.4	24	23.7	20.2	23.6	31.3	24.6
Ce	40.6	47.2	45.4	43.1	51.2	51.8	48.9	43.4	50	64.3	51
Pr	4.42	4.94	4.84	4.82	5.64	5.43	5.22	4.61	5.4	6.95	5.68
Nd	16.5	17.6	17.2	18.1	20.9	20.1	19	16.9	19.8	25.4	20.4
Sm	3.43	3.18	3.14	3.57	4.11	3.89	3.73	3.44	3.89	4.66	4.18
Eu	0.45	0.36	0.41	0.5	0.53	0.53	0.51	0.5	0.51	0.57	0.5
Gd	3.19	2.64	2.73	3.66	3.8	3.68	3.44	3.05	4.02	4.28	3.71
Tb	0.54	0.39	0.43	0.61	0.61	0.58	0.55	0.5	0.68	0.67	0.62
Dy	3.32	2.2	2.48	3.92	3.66	3.18	3.24	2.99	4.11	4	3.68
Ho	0.67	0.41	0.49	0.8	0.67	0.62	0.62	0.58	0.81	0.76	0.7
Er	2.17	1.4	1.57	2.65	2.21	1.94	2.08	1.84	2.71	2.43	2.24
Tm	0.34	0.23	0.26	0.43	0.37	0.31	0.32	0.28	0.43	0.37	0.37
Yb	2.55	1.64	1.91	3.05	2.6	2.26	2.25	2.03	3.04	2.7	2.68
Lu	0.39	0.26	0.32	0.44	0.4	0.34	0.35	0.31	0.47	0.42	0.41
Zr	104	110	103	116	116	112	118	108	105	115	112
Hf	4.2	4.36	4.17	4.2	4.45	4.24	4.19	4.24	4.11	4.49	4.29
Sc	4.66	3.39	4.24	5.1	5.51	5.01	6.24	4.16	5.05	5.16	7.85
Ga	17.8	16.4	17.6	18	17.8	17.7	19.1	17.5	17.7	19.4	22.3
Rb	363	309	345	367	305	303	326	331	436	428	363
Sr	109	96.5	104	87.7	146	147	128	136	68.8	96.7	116
Nb	16.7	26.2	36.6	15.5	15.7	17.7	19.3	15.5	16	17.8	16.6
Cs	25.9	24	26.9	26.6	21	21.2	26.6	23	26	25.8	34.1
Ba	323	281	307	244	328	361	346	384	262	332	276
Ta	2.26	4.71	7.13	1.87	2.09	2.43	2.24	1.98	2.04	2.05	1.84
Pb	20.2	23.9	18.5	21	23.5	24.5	22.2	23.7	23.2	25	18.9
Th	20.4	16.7	15.9	19.8	19.8	21.8	21.9	18.7	18.1	22.9	19.5
U	5.56	5.77	5.76	6.22	6.42	5.69	4.77	5.26	6.96	5.17	7.11

like, magmatic signature for the early vein stages (including molybdenite), whereas later vein stages (containing chalcopyrite) recorded greater crustal signature. Combined with the regional geological history, we conclude that the evolution of the porphyry Mo deposit in the Donggebi area and associated Mo mineralization during early Mesozoic time were closely related to a post-collisional extensional setting.

Acknowledgements

We are indebted to Bin Cui, Jingwen Mao, Kezhang Qin, Zhaochong Zhang, Yitian Wang, Jinyi Li, Tianlin Ma, Lian-Chang Zhang, Zhiliang Wang, and Jianming Yang for discussions on this manuscript. Many of the ideas in this paper were initiated and rectified during these discussions. This study was financially supported by funds from the National Key R&D Program of China (2017YFC0601206), the NSFC Project (41772078, 40725009, 40421303, and 40572043), the State Key Laboratory of Lithospheric Evolution, the Chinese State 973 Project (2001CB409801) and Hong Kong RGC (7066/07P). This paper is a contribution to the ILP (ERAS) and IGCP 480.

References

Allen, M.B., Windley, B.F., Zhang, C., 1993. Palaeozoic collisional tectonics and magmatism of the Chinese Tien Shan, central Asia. Tectonophysics 220, 89–115.

Badarch, G., Cunningham, W.D., Windley, B.F., 2002. A new terrane subdivision for Mongolia: implications for the Phanerozoic crustal growth of Central Asia. J. Asian Earth Sci. 21, 87–110.

Berzina, A.N., Sotnikov, V.I., Economou-Eliopoulos, M., Eliopoulos, D.G., 2005. Distribution of rhenium in molybdenite from porphyry Cu-Mo and Mo-Cu deposits of Russia (Siberia) and Mongolia. Ore Geol. Rev. 26, 91–113.

Chen, Y.J., Zhang, C., Wang, P., Franco, P., Li, N., 2017. The Mo deposits of Northeast China. A powerful indicator of tectonic settings and associated evolutionary trends. Ore Geol. Rev. 81, 602–640.

Chen, B., Jahn, B.M., Tian, W., 2009. Evolution of the Solonker suture zone: constraints from zircon U-Pb ages, Hf isotopic ratios and whole-rock Nd–Sr isotope compositions of subduction- and collision-related magmas and forearc sediments. J. Asian Earth Sci. 34, 245–257.

Coleman, R., 1989. Continental growth of Northwest China. Tectonics 8, 621–635.

Deng, F.Y., 2012. Magma rocks of geochemistry characteristics s of East Gobi molybdenum mine in Hami, Xinjiang. Western Explor. Eng. 3, 115–119 (in Chinese with English abstract).

Deng, X.H., Wang, J.B., Pirajno, F., Wang, Y.W., Li, Y.C., Li, C., Zhou, L.M., Chen, Y.J., 2016. Re-Os dating of chalcopyrite from selected mineral deposits in the Kalatag district in the eastern Tianshan Orogen, China. Ore Geol. Rev. 77, 72–81.

Deng, X.H., Chen, Y.J., Santosh, M., Wang, J.B., Li, C., Yue, S.W., Zheng, Z., Chen, H.J., Tang, H.S., Dong, L.H., Qu, X., 2017. U-Pb zircon, Re-Os molybdenite geochronology and Rb-Sr geochemistry from the Xiaobaishitou W (-Mo) deposit. implications for Triassic tectonic setting in eastern Tianshan,NW China. Ore Geol. Rev. 80, 332–351.

Delibaş, O., 2009, The role of magma mixing processes in the formation of iron, copper, molybdenum and lead mineralizations of Kırıkkale-Yozgat region (Ph. D. thesis). Hacettepe University, Turkey, p. 210.

Delibaş, O., Genc, Y., Decampos, C. P., 2011, Magma mixing and unmixing related mineralization in the Karacaali Magmatic Complex. In: Sial, A.N., Bettencourt, J.S., Decampos, C.P., Ferreira, V.P. (eds.), Granite-related ore deposits. Geological Society Special Publications, London, vol. 350, pp. 149–173.

Ding, T.P., Valkiers, S., Wang, D.F., Bai, R.M., Zou, X.Q., Li, Y.H., Zhang, Q.L., De Bievre, P., 2001. The δ32S and δ34S values and absolute 32S/33S and 32S/34S ratios of IAEA and Chinese sulfur isotope reference materials. Bull. Mineral. Petrol. Geochem. 20, 425–427 (in Chinese with English abstract).

Du, A.D., He, H.L., Yin, N.W., 1995. A study of the rhenium-osmium geochronometry of molybdenites. Acta Geol. Sin. 8, 171–181 (in Chinese with English abstract).

Du, A.D., Wang, S.X., Sun, W.D., Zhang, D., Liu, D., 2001, Precise Re-Os dating of molybdenite using Carius tube, NTIMS and ICPMS. In. Piestrzynski et al (eds.) Mineral Deposits at the 21st Century, pp. 405–407.

Gao, J., Klemd, R., Zhu, M.T., Li, J.L., Bo Wan, B., Xiao, W.J., Qingdong Zeng, Q.D., Shen, P., Sun, J.G., Qin, K.Z., Campose, E., 2018. Large-scale porphyry-type mineralization in the Central Asian metallogenic domain: A review. J. Asian Earth Sci. 165, 7–36.

Goldfarb, R.J., Taylor, R.D., Collins, G.S., Goryachev, N.A., Orlandini, O.F., 2013. Phanerozoic continental growth and gold metallogeny of Asia. Gondwana Res. 25, 48–102.

Guo, F., 2000. Affinity between Palaeozoic blocks of Xinjiang and their suturing ages. Acta Geol. Sin. 74, 1–6.

Han, C.M., Xiao, W.J., Zhao, G.C., Mao, J.W., Li, S.Z., Yan, Z., Mao, Q.G., 2006. Major types, characteristics and geodynamic mechanism of Late Paleozoic copper deposits in Northern Xinjiang, Northwestern China. Ore Geol. Rev. 28, 308–328.

Han, C.M., Xiao, W.J., Zhao, G.C., Sun, M., Qu, W.J., Du, A.D., 2010. In-Situ U-Pb, Hf and Re-Os isotopic analyses of the Xiangshan Ni-Cu-Co deposit in Eastern Tianshan (Xinjiang), Central Asia Orogenic Belt. constraints on the timing and genesis of the mineralization. Lithos 120, 547–562.

He, G.Q., Li, M.S., Liu, D.Q., Zhou, N.H., 1994, Palaeozoic Crustal Evolution and Mineralization in Xinjiang of China. Urumqi, Xinjiang People's Publishing House, pp. 1–437.

Huang, C.Y., Wu, B.Y., Weng, J.C., Li, W.Z., Xi, G.Z., Yuan, D.F., Zhao, X.B., 2011a. Discovery of the Eastern Gobi Hugesize Molybdenum Ore Deposit and Its Prospecting Significance in Eastern Tianshan. Geol. Survey Res. 34, 169–188 (in Chinese with English abstract).

Huang, C.Y., Lang, Y.F., Dong, L.Q., Fu, Z.G., 2011b. Geological characteristics and genesis of the the Donggebi oversize molybdenum deposit in Eastern Tianshan. China Molybdenum Indust. 35, 8–17 (in Chinese with English abstract).

Jahn, B.-M., Wu, F.-Y., Chen, B., 2000. Granitoids of the Central Asian Orogenic Belt and continental growth in the Phanerozoic. Transactions of the Royal Society of Edinburgh. Earth Sci. 91, 181–193.

Jahn, B.M., Litvinovsky, B.A., Zanvilevich, A.N., Reichow, M., 2009. Peralkaline granitoid magmatism in the Mongolian-Transbaikalian Belt: Evolution, petrogenesis and tectonic significance. Lithos 113, 521–539.

Ji, J.S., Tao, H.X., Zeng, Z.R., Li, H.Q., Zhang, L.C., 1994. Geology of the Kanggurtag Gold Mineralization Zone and Exploration. Geological Publishing House, East Tianshan, Beijing, pp. 136.

Kovalenko, V.I., Yarmolyuk, V.V., Kovach, V.P., Kotov, A.B., Kozakov, I.K., Salnikova, E.B., Larin, A.M., 2004. Isotope provinces, mechanisms of generation and sources of the continental crust in the Central Asian mobile belt. Geological and isotopic evidence. J. Asian Earth Sci. 23, 605–627.

Lamb, M.A., Badarch, G., Navratil, T., Poier, R., 2008. Structural and geochronologic data from the Shin Jinst area, eastern Gobi Altai, Mongolia: implications for Phanerozoic intracontinental deformation in Asia. Tectonophysics 451, 312–330.

Laurent-Charvet, S., Charvet, J., Monie, P., Shu, L., 2003. Late Paleozoic strike-slip shear zones in eastern central Asia (NW China): new structural and geochronological data. Tectonics 22, 1009.

Liu, D.Q., Chen, Y.C., Wang, D.H., 2003. A discussion on problems related to mineralisation of Tuwu-Yandong Cu-Mo ore field in Hami, Xinjiang. Min. Deposits 22, 334–344 (in Chinese with English abstract).

Li, W., Jackson, S.E., Pearson, N.J., Graham, S., 2010. Copper isotopic zonation in the Northparkes porphyry Cu-Au deposit, SE Australia. Geochim. Cosmochim. Acta 74, 4078–4096.

Li, X.H., Liu, Y., Li, Q.L., Guo, C.H., Chamberlain, K.R., 2009, Precise determination of Phanerozoic zircon Pb/Pb age by multi-collector SIMS without external standardization. Geochem. Geophys. Geosyst. 10, Q04010. doi:10.1029/cGC002400.

Ludwig, K.R., 2001, User's manual for Isoplot/Ex (rev. 2.49). A geochronological toolkit for Microsoft Excel. Berkeley Geochronology Center Special Publication 1, 1–55.

Ma, R.S., Shu, L.S., Sun, J., 1997. Tectonic Evolution and Metallogeny of Eastern Tianshan Mountains. Geological Publishing House, Beijing, pp. 202.

Mao, J.W., Zhang, Z.H., Zhang, Z.C., Du, A.D., 1999. Re-Os isotopic dating of molybdenites in the XiaoliugouW(Mo) deposit in the Northern Qilian mountains and its geological significance. Cheochimica et Cosmochimica Acta 63, 1815–1818.

Mao, J.W., Yang, J.M., Qu, W.J., Du, A.D., Wang, Z.L., Han, C.M., 2002. Re-Os age of Cu-Ni ores from the Huangshandong Cu-Ni sulfide deposit in the East Tianshan Mountains and its implication for geodynamic processes. Min. Deposits 21, 323–330 (in Chinese with English abstract).

Mao, J.W., Pirajno, F., Cook, N., 2011. Mesozoic metallogeny in East China and corresponding geodynamic settings-An introduction to the special issue. Ore Geol. Rev. 43, 1–7.

Mao, J.W., Du, A.D., Seltmann, R., Yu, J.J., 2003. Re-Os ages for the Shameika porphyry Mo deposit and the Lipovy Lograre metal pegmatite, central Urals, Russia. Minerlium Deposita 38, 251–257.

Mao, J.W., Xie, G.Q., Zhang, Z.H., Li, X.F., Wang, Y.T., Zhang, C.Q., Li, Y.F., 2005. Mesozoic large-scale metallogenic pulses in North China and corresponding geodynamic settings. Acta Petrologica Sinica 21, 169–188 (in Chinese with English abstract).

Mao, J.W., Wang, Y.T., Bernd, L., Yu, J.J., Du, A.D., Mei, Y., Li, Y.F., Zang, W., Stein, H.J., Zhou, T.F., 2006. Molybdenite Re-Os and albite 40Ar/39Ar dating of Cu-Au-Mo and magnetite porphyry systems in the Yangtze River valley and metallogenic implications. Ore Geol. Rev. 29, 307–324.

Markey, R., Stein, H., Morgan, J., 1998. Highly precise Re-Os dating for molybdenite using alkaline fusion and NTIMS. Talanta 45, 935–946.

Orolmaa, D., Erdenesaihan, G., Borisenko, A.S., Fedoseev, G.S., Babich, V.V., Zhmodik, S.M., 2008. Permian-Triassic granitoid magmatism and metallogeny of the Hangayn (central Mongolia). Russ. Geol. Geophys. 49, 534–544.

Seltmann, R., Porter, T.M., 2005, The porphyry Cu-Au/Mo deposits of Central Eurasia. 1. Tectonic, geologic and metallogenic setting and significant deposits. In: Porter, T.M. (ed.), Super Porphyry Copper and Gold Deposits. A Global Perspective. PGC Publishing, Adelaide 2, pp. 467–512.

Seltmann, R., Mike Porter, T., Pirajno, F., 2014. Geodynamics and metallogeny of the central Eurasian porphyry and related epithermal mineral systems. A review. J. Asian Earth Sci. 79, 810–841.

Şengör, A.M.C., Natal'in, B.A., Burtman, U.S., 1993. Evolution of the Altaid tectonic collage and Paleozoic crustal growth in Eurasia. Nature 364, 209–304.

Şengör, A.M.C., Natal'in, B.A., 1996. Turkic-type orogeny and its role in the making of the continental crust. Annu. Rev. Earth Planet. Sci. 24, 263–337.

Shirey, S.B., Walker, R.J., 1995. Carius tube digestion for low-bank rhenium-osmium analysis. Anal. Chem. 67, 2136–2141.

Smoliar, M.I., Warker, R.J., Morgan, J.W., 1996. Re-Os ages of group IIA, IIIA, IVA and VIB iron meteorites. Science 271, 1099–1102.

Stacey, J.S., Kramers, J.D., 1975. Approximation of terrestrial lead isotope evolution by a two-stage model. Earth Planet. Sci. Lett. 26, 207–221.

Stein, H.J., Markey, R.J., Morgan, J.W., Du, A.D., Sun, Y.L., 1997. Highly precise and

accurate Re-Os ages for molybdenite from the East Qinling molybdenium belt, Shaanxi Province, China. Econ. Geol. 92, 827–835.
Tu, L.Q., Ma, Y.F., Shi, S.R., Yin, J.F., Tu, J.F., 2011. Geological and wall-rock alteration characteristics of the Donggebi deposit, Hami City. Xinjiang Geol. 29, 433–436 (in Chinese with English abstract).
Ueda, A., Sakai, H., 1984. Sulfur isotope study of Quaternary volcanic rocks from the Japanese Islands arc. Geochim. Cosmochim. Acta 48, 1837–1848.
Wang, Y., Sun, G., Li, J., 2010. U-Pb (SHRIMP) and 40Ar/39Ar geochronological constraints on the evolution of the Xingxingxia shear zone, NW China: a Triassic segment of the Altyn Tagh fault system. Geol. Soc. Am. Bull. 122, 487–505.
Wang, B., 2011. Geological characteristics and prospecting types of East Gobi molybdenum mine in Hami. China Molybdenum Indust. 35, 7–10 (in Chinese with English abstract).
Wiedenbeck, M., Alle, P., Corfu, F., Griffin, W.L., Meier, M., Oberli, F., Vonquadt, A., Roddick, J.C., Speigel, W., 1995. Three natural zircon standards for U-Th-Pb, Lu-Hf, trace element and REE analyses. Geostand. Newslett. 19, 1–23.
Windley, B.F., Allen, M.B., Zhang, C., Zhao, Z.Y., Wang, G.R., 1990. Paleozoic accretion and Cenozoic re-deformation of the Chinese Tien Shan Range, Central Asia. Geology 18, 128–131.
Windley, B.F., Alexeiev, D., Xiao, W.J., Kröner, A., Badarch, G., 2007. Tectonic models for accretion of the Central Asian Orogenic Belt. J. Geol. Soc. 64, 31–47.
Wu, F.Y., Jahn, B.M., Wilde, S., Sun, D.Y., 2000. Phanerozoic crustal growth. U-Pb and Sr-Nd isotopic evidence from the granites in northeastern China. Tectonophysics 328, 89–113.
Wu, F.Y., Sun, D.Y., Li, H., Jahn, B.-M., Wilde, S., 2002. A-type granites in northeastern China. age and geochemical constraints on their petrogenesis. Chem. Geol. 187, 143–173.
Wu, F.Y., Yang, Y.H., Xie, L.W., Yang, J.H., Xu, P., 2006. Hf isotopic compositions of the standard zircons and baddeleyites used in U-Pb geochronology. Chem. Geol. 234, 105–126.
Wu, F.Y., Sun, D.Y., Ge, W.C., Zhang, Y.B., Grant, M.L., Wilde, S.A., Jahn, B.M., 2011. Geochronology of the Phanerozoic granitoids in northeastern China. J. Asian Earth Sci. 41, 1–30.
Wu, Y.S., Chen, Y.J., Zhou, K.F., 2017a. Mo deposits in Northwest China. Geology, geochemistry, geochronology and tectonic setting. Ore Geol. Rev. 81, 641–671.
Wu, Y.S., Zhou, K.F., Li, N., Chen, Y.J., 2017b. Zircon U-Pb dating and Sr–Nd–Pb–Hf isotopes of the ore-associated porphyry at the giant the Donggebi Mo deposit, Eastern Tianshan, NW China. Ore Geol. Rev. 81, 794–807.
Wu, Y.S., Wang, P., Yang, Y.F., Xiang, N., Li, N., Zhou, K.F., 2014. Ore geology and fluid inclusion study of the the Donggebi giant porphyry Mo deposit, Eastern Tianshan, NW China. Geol. J. 49, 559–573.
Xiao, W.J., Zhang, L.C., Qin, K.Z., Sun, S., Li, J.L., 2004a. Paleozoic accretionary and collisional tectonics of the Eastern Tianshan (China). Implications for the continental growth of central Asia. Am. J. Sci. 304, 370–395.
Xiao, W.J., Windley, B.F., Hao, J., Zhai, M.G., 2003, Accretion leading to collision and the Permian Solonker suture, Inner Mongolia, China. termination of the Central Asian orogenic belt. Tectonics 22, 069, doi:10.1029/2002TC1484.
Xiao, W.J., Windley, B.F., Badarch, G., Sun, S., Li, J.L., Qin, K.Z., Wang, Z.H., 2004b. Palaeozoic accretionary and convergent tectonics of the southern Altaids. implications for the lateral growth of Central Asia. J. Geol. Soc., London 161, 339–342.
Xiao, W., Windley, B.F., Hao, J., Zhai, M., 2003b. Accretion leading to collision and the Permian Solonker suture, Inner Mongolia, China. Termination of the central Asian orogenic belt. Tectonics 22 (6), 1–20.
Xiao, W., Kroner, A., Windley, B., 2009. Geodynamic evolution of Central Asia in the Paleozoic and Mesozoic. Int. J. Earth Sci. 98, 1185–1188.
Yarmolyuk, V.V., Kovalenko, V.I., Sal'nikova, E.B., Budnikov, S.V., Kovach, V.P., Kotov, A.B., Ponomarchuk, V.A., 2002. Tectono-Magmatic zoning, magma sources and geodynamics of the early Mesozoic Mongolia-Trasbaikal province. Geotectonics 36, 293–311.
Yang, Z.Q., Wu, B.Y., Zheng, S.S., An, J.L., Chang, Y.Q., 2011. Geological and geochemistical characteristics of ore-forming granite porphyry in East Gobi porphyry molybdenum deposit in Xinjiang. Geol. Min. Resources South China 27, 208–214 (in Chinese with English abstract).
Zhang, H.T., So, C.S., Yun, S.T., 1999. Regional geologic setting and metallogenesis of central Inner Mongolia, China. Guides for exploration of mesothermal gold deposits. Ore Geol. Rev. 14, 129–146.
Zhang, L.C., Liu, T.B., Shen, Y.C., 2002. Isotopic geochronology of the Late Paleozoic Kangguer gold deposits of East Tianshan Mountains, Xinjiang, NW China. Resour. Geol. 52, 249–261.
Zhang, L.C., Xiao, W.J., Qin, K.Z., Qu, W.J., Du, A.D., 2005a. Re-Os isotopic dating of molybdenite and pyrite in the Baishan Mo-Re deposit, eastern Tianshan, NW China, and its geological significance. Miner. Deposita 39, 960–969.
Zhang, Z.Z., Gu, L.X., Wu, C.Z., Li, W.Q., Xi, A.H., Wang, S., 2005b. Zircon SHRIMP dating for the Weiya pluton, eastern Tianshan: its geological implications. Acta Geologica Sinica (English Edition) 79, 481–490.